SCALABLE ELEMENT-WISE FINITE-TIME OPTIMIZATION FOR DEEP NEURAL NETWORKS

Anonymous authors
Paper under double-blind review

ABSTRACT

Optimization algorithms are fundamental to deep neural network training, where exponential growth from millions to hundreds of billions of parameters has made training acceleration a critical necessity. While adaptive methods like Adam achieve remarkable success through element-wise learning rates, understanding their continuous-time counterparts can provide valuable theoretical insights into convergence guarantees beyond asymptotic rates. Recent advances in continuous-time optimization have introduced fixed-time stable methods that promise finite-time convergence independent of initial conditions. However, existing approaches like FxTS-GF suffer from dimensional coupling, where coordinate updates depend on global gradient norms, creating suboptimal scaling in high-dimensional problems typical of deep learning. To address this issue, we introduce an element-wise finite-time optimization framework that eliminates dimensional coupling through coordinate-independent dual-power dynamics. Furthermore, we extend the framework to momentum-enhanced variants for deep model training while preserving convergence properties through continuous-time analysis. Under mild assumptions, we establish rigorous finite-time and fixed-time convergence guarantees. Notably, our framework reveals that widely-used sign-based optimizers like SignSGD and Signum emerge as limiting cases, providing theoretical grounding for their empirical effectiveness. Experiments on CIFAR-10/100 and C4 language modeling demonstrate consistent improvements over existing methods.

1 INTRODUCTION

Optimization algorithms are the cornerstone of deep neural network training, determining both the feasibility and efficiency of learning in large-scale models. As neural networks have grown exponentially, training acceleration has evolved from a convenience to a critical necessity, where a single large language model(LLM) can require thousands of GPU-hours and cost millions of dollars to train. This computational reality has driven decades of intensive research into faster optimization methods. The journey began with stochastic gradient descent (SGD), the foundational algorithm that enabled neural network training, followed by momentum-based acceleration techniques like heavy-ball momentum (Polyak, 1964) and Nesterov acceleration (Nesterov, 1983) that significantly improved convergence rates.The development of adaptive methods marked a major breakthrough: AdaGrad (Duchi et al., 2011) introduced coordinate-wise learning rates, RMSprop improved upon this with exponential moving averages, while Adam (Kingma & Ba, 2014) combined both first and second moment estimation and AdamW (Loshchilov & Hutter, 2017) which decouples weight decay. More recent advances include second-order methods like Shampoo (Gupta et al., 2018) that use full preconditioning matrices, and Sophia (Liu et al., 2023) which efficiently approximates Hessian information for LLM training representing the current pinnacle of discrete optimization approaches.

However, the optimization methods described above are fundamentally designed from a discrete-time perspective, focusing on iterative parameter updates with step-by-step convergence analysis. While this discrete viewpoint has achieved remarkable practical success, it inherently limits the theoretical frameworks available for convergence analysis. In contrast, continuous-time optimization theory offers fundamentally different analytical tools through dynamical systems theory that can provide stronger convergence guarantees. Recent advances have introduced finite-time and fixed-time stability concepts (Bhat & Bernstein, 2000; Polyakov, 2011), where systems reach equilibrium exactly within bounded time horizons, with fixed-time variants providing bounds independent of

initial conditions. The pioneering work by Budhraja et al. (2022) first applied these concepts to optimization and deep learning model training, introducing fixed-time stable gradient flows (FxTS-GF), employing dynamics of the form:

$$\dot{\mathbf{w}}(t) = -c_1 \frac{\nabla \mathcal{L}(\mathbf{w})}{\|\nabla \mathcal{L}(\mathbf{w})\|^{\frac{\mathbf{p_1-2}}{\mathbf{p_1-1}}}} - c_2 \frac{\nabla \mathcal{L}(\mathbf{w})}{\|\nabla \mathcal{L}(\mathbf{w})\|^{\frac{\mathbf{p_2-2}}{\mathbf{p_2-1}}}}, \tag{1}$$

where $c_1, c_2 > 0$, $p_1 > 2$ and $p_2 \in (1, 2)$, which demonstrated superior performance than Adam in solving the Rosenbrock function and training shallow neural networks model using the MNIST dataset. While these methods provide elegant theoretical guarantees, the global norm $\|\nabla \mathcal{L}(\mathbf{w})\|$ creates dimensional coupling that becomes problematic in large-scale settings. In high-dimensional networks, this global normalization is dominated by the largest gradient components, diminishing updates for smaller but potentially crucial gradients. This limitation highlights a critical gap between control-theoretic optimization and practical deep learning requirements. In contrast, the remarkable success of Adam-family optimizers in deep learning stems from their element-wise adaptivity, where each parameter maintains its own learning rate based on local gradient statistics. This design philosophy naturally handles the heterogeneous optimization landscape and has proven essential for training neural networks, especially for transformer-based models (Zhang et al., 2024a).

Motivated by this insight, we ask: *Can we bring the theoretical rigor of finite/fixed-time optimization to large-scale deep learning by adopting element-wise design principles?*

We introduce an element-wise finite-time optimization framework specifically designed for the challenges of large-scale neural network training:

$$\dot{\mathbf{w}} = -c_1 \operatorname{sign}(\mathbf{g}) \odot |\mathbf{g}|^{p_2} - c_2 \operatorname{sign}(\mathbf{g}) \odot |\mathbf{g}|^{2-p_1}, \tag{2}$$

where $\mathbf{g} = \nabla \mathcal{L}(\mathbf{w})$ is the gradient of the objective function $\mathcal{L}(\mathbf{w})$, $c_1, c_2 > 0$, $p_1 < 2$ and $p_2 \in (0, 1)$, $\odot$ denote the element-wise operations. This design eliminates dimensional coupling by making each coordinate evolve independently, preserving the element-wise adaptivity crucial for deep learning while maintaining rigorous convergence guarantees from control theory. Our framework reveals a remarkable theoretical bridge between control-theoretic optimization and practical deep learning methods. When parameters approach certain limits ($p_1 \to 2$, $p_2 \to 0$), our dynamics reduce to SignSGD (Bernstein et al., 2018). This connection suggests that successful sign-based optimizers used in practice are actually principled approximations of theoretically grounded finite/fixed-time gradient flows. Our contributions are as follows:

1. **Element-wise finite/fixed-time optimization framework**: We introduce the scalable finite-time optimization method that eliminates dimensional coupling through coordinate-independent dynamics, enabling rigorous finite-time convergence guarantees for high-dimensional deep learning while preserving element-wise adaptivity.
2. **Momentum-enhanced variants with theoretical guarantees**: We extend our framework to incorporate exponential moving averages and Polyak momentum for stochastic training, establishing explicit finite-time and fixed-time convergence results under standard smoothness and Polyak-Łojasiewicz conditions.
3. **Theoretical unification of sign-based optimizers**: We show that widely used distributed training optimizers SignSGD and Signum emerge as limiting cases of our method, providing theoretical foundation for their empirical effectiveness in large-scale model training.

2 Related Work

Deep Learning Optimization: The success of large-scale neural network training fundamentally relies on adaptive optimization methods that adjust learning rates based on gradient statistics. This paradigm began with AdaGrad (Duchi et al., 2011), which introduced coordinate-wise learning rates by accumulating squared gradients, and was further developed by the Adam family of optimizers (Kingma & Ba, 2014; Loshchilov & Hutter, 2017). Adam combines first and second moment estimation with exponential moving averages, while AdamW decouples weight decay from gradient-based updates, and AdaBelief (Zhuang et al., 2020) refines second-moment estimation to better capture gradient predictability, leading to their widespread adoption across various deep learning applications. Adam's widespread adoption across deep learning applications (Orvieto & Gower, 2025)

reflects its consistent performance advantages over SGD, particularly pronounced in transformer architectures. Recent theoretical work by Zhang et al. (Zhang et al., 2024a) explains this effectiveness by analyzing transformer Hessian structures, revealing significant coordinate heterogeneity where different parameters experience vastly different curvature properties. This heterogeneous structure necessitates coordinate-specific learning rates, providing theoretical justification for element-wise adaptive methods. Dong et al. (2025) further quantify this heterogeneous structure, establishing rigorous mathematical foundations for adaptive optimization's empirical success. The principle of heterogeneity-aware optimization has manifested in various forms across the field's development. Earlier work like LAMB (You et al., 2019) recognized that different network depths require distinct optimization strategies, extending adaptive principles to layer-wise normalization for effective large-batch training of transformers. More recently, Adam-mini (Zhang et al., 2024b) explicitly exploits the block-diagonal structure of neural network Hessians, assigning learning rates per dense sub-block while maintaining computational efficiency. These methods demonstrate that the key insight extends beyond simple element-wise adaptation to various forms of structured, heterogeneity-aware optimization. More recent advances continue to push the boundaries of adaptive optimization. Advanced preconditioning methods like Shampoo (Gupta et al., 2018) and SOAP (Vyas et al., 2024) implement block-diagonal preconditioning matrices, while ASGO (An et al., 2025) introduces adaptive structured gradient optimization. Second-order approaches like Sophia (Liu et al., 2023) efficiently approximate Hessian information specifically for large language model training. For distributed training of large models, sign-based methods like SignSGD, Signum (Bernstein et al., 2018), and Lion (Chen et al., 2023) maintain adaptive characteristics while providing communication efficiency.

Finite-Time and Fixed-Time Optimization Theory: The theory of finite-time stability has its roots in control systems, where Bhat & Bernstein (2000) established fundamental results for systems that reach equilibrium in finite time rather than asymptotically. Polyakov Polyakov (2011) extended this framework to fixed-time stability, providing uniform convergence bounds independent of initial conditions, which is particularly valuable for control applications with strict timing requirements. These theories are then extended to the optimization Garg & Panagou (2021), and distributed optimization Chen & Li (2018), with applications on multi-agent system and ummaned autonomus system Liu et al. (2022). In Nguyen et al. (2022), the fixed time convergence theory is further extended to systems with time-varying coefficients. These methods demonstrate extraordinary acceleration in small-scale continuous systems, whereas their application in the deep learning field remains largely unexplored. Recently, these theoretical advances have recently been applied to machine learning and deep learning problems. Budhraja et al. (2022) introduced fixed-time stable gradient flows (FxTS-GF) for convex optimization , demonstrating how control-theoretic concepts can provide stronger convergence guarantees than classical gradient descent.

3 Problem Formulation and Theoretical Framework

Consider the unconstrained optimization problem:

$$\min_{\mathbf{w}\in\mathbb{R}^d} \mathcal{L}(\mathbf{w}) \tag{3}$$

where $\mathcal{L} : \mathbb{R}^d \to \mathbb{R}$ is continuously differentiable with global minimum $\mathbf{w}^*$ and optimal value $\mathcal{L}^* = \mathcal{L}(\mathbf{w}^*)$. Classical approaches to solving problem (3) include first-order and second-order methods. Gradient descent employs the update rule $\mathbf{w}_{k+1} = \mathbf{w}_k - \eta\nabla\mathcal{L}(\mathbf{w}_k)$ and offers simplicity but exhibits slow linear convergence rates under strong convexity. The discrete-time algorithms can be interpreted as dynamical system, while its continuous-time counterparts, derived by considering infinitesimal step sizes, take the form of differential equations, i.e.

$$\dot{\mathbf{w}}(t) = -\nabla\mathcal{L}(\mathbf{w}(t)). \tag{4}$$

Analyzing the continuous-time system can provide valuable theoretical insights, such as stability properties and convergence rates, offering a complementary perspective to discrete optimization analysis. Both classical discrete methods and their continuous-time counterparts provide only asymptotic convergence guarantees: the objective function approaches the optimum as time or iterations tend to infinity, but never reaches it exactly in finite time. Recent advances in optimization theory have introduced stronger convergence concepts that go beyond asymptotic guarantees. These developments draw from the stability theory of dynamical systems to provide finite-time and fixed-time convergence guarantees, with definitions given as Definition 1, 2.

Definition 1 (Finite-Time Stability Bhat & Bernstein (2000)). *A dynamical system $\dot{x} = f(x)$ with equilibrium at $x = 0$ is finite-time stable if there exists a settling time function $T : \mathbb{R}^n \to \mathbb{R}_+$ such that for any initial condition $x(0) = x_0$, the solution satisfies $x(t) = 0$ for all $t \geq T(x_0)$.*

Definition 2 (Fixed-Time Stability Polyakov (2011)). *A finite-time stable system is fixed-time stable if the settling time function $T(x_0)$ is globally bounded:* $\sup_{x_0 \in \mathbb{R}^n} T(x_0) < \infty$.

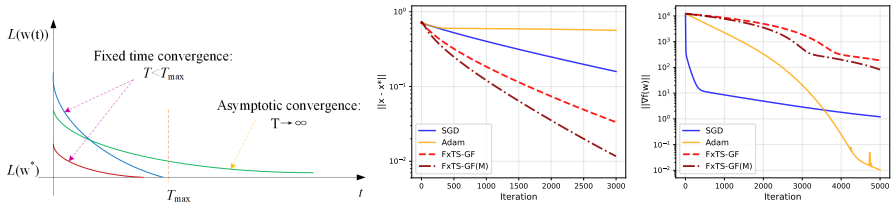

(a) (b) (c)

Figure 1: (a) Fixed time convergence vs asymptotic convergence, (b) Convergence result for minimizing Rosenbrock function with various optimization methods, where fixed time methods converge faster than SGD and Adam, (c) Convergence result for small-scale quadratic problem with various optimization methods, where Adam converge faster than fixed time methods.

The key advantage of fixed-time stability is that convergence time is independent of initial conditions, providing stronger guarantees than classical finite-time stability, as demonstrated in Figure 1a. Designing finite/fixed time gradient flow normally involves the following lemmas:

Lemma 1 (Bhat & Bernstein (2000)). *Let $V(t)$ be absolutely continuous and satisfy $\dot{V}(t) \leq -\alpha V(t)^\gamma$ for $\alpha > 0$ and $\gamma \in (0, 1)$. Then $V(t)$ reaches zero in finite time $T^* < \infty$ given by $T^* \leq \frac{V(0)^{1-\gamma}}{\alpha(1-\gamma)}$.*

Lemma 2 (Polyakov (2011)). *Consider a Lyapunov function $V(\mathbf{w}) \geq 0$ with $V(\mathbf{w}) = 0$ if and only if $\mathbf{w} = \mathbf{w}^*$. If there exist constants $a, b > 0$, $0 < \alpha < 1 < \beta$ such that$\dot{V} \leq -aV^\alpha - bV^\beta$, then the system is fixed-time stable with settling time bounded by $T \leq \frac{1}{a(1-\alpha)} + \frac{1}{b(\beta-1)}$.*

Followed by Lemma 1, 2, different control laws are designed to achieve the finite time or fixed time convergence. However, existing finite/fixed-time optimization methods, including FxTS-GF(M) (shown in (1)), encounter fundamental scalability limitations due to dimensional coupling that severely impede their adoption in large-scale machine learning. To demonstrate this property, we adopt the set from (Budhraja et al., 2022) with Rosenbrock function $f(x_1, x_2) = (1 - x_1)^2 + 100(x_2 - x_1^2)^2$,and analyze the generic quadratic minimization problem, $f(x) = \frac{1}{2} w^T H w$, where $H = \text{diag}(H_1, H_2, H_3)$ is a block-diagonal, positive-definite matrix. Let $D_i = \dim(w_i)$ be the number of parameters in block i. Specifically, theheterogeneity by drawing eigenvalues for H_1, H_2, and H_3 from $\{0.1, 0.2, 1.5, 3\}$, $\{49, 50, 51, 100\}$, and $\{1000, 1100, 2001, 2005\}$, respectively, the size of each block is set to 50. Fig. 1b and 1c demonstrate that the FxTS-GF outperforms Adam and SGD on Tiny Resenbrock function but fails with a small-scale quadratic problem with heterogeneous eigenvalues.

4 Methodology

4.1 Element-wise Finite-Time Optimization Framework

To address the dimensional coupling limitations of existing finite-time methods, we propose an element-wise approach that enables coordinate-independent convergence analysis. Our core insight is to replace global gradient norms with element-wise operations, yielding the dynamics:

$$\dot{\mathbf{w}} = -c_1 \operatorname{sign}(\mathbf{g}) \odot |\mathbf{g}|^{p_2} - c_2 \operatorname{sign}(\mathbf{g}) \odot |\mathbf{g}|^{2-p_1}, \tag{5}$$

where $\mathbf{g} = \nabla \mathcal{L}(\mathbf{w})$, constants $c_1, c_2 > 0$, exponents $p_2 \in (0, 1)$, $p_1 \in (0, 2)$, and $\odot$ denotes element-wise multiplication. This formulation eliminates the global coupling present in methods like FxTS-GF while preserving the dual-power structure essential for finite-time convergence.

The key theoretical advantage lies in the coordinate-wise nature of the dynamics: each parameter w_i evolves according to its local gradient information g_i, avoiding the dimensional scaling issues that plague globally-coupled approaches.

Assumption 1. *The objective function $\mathcal{L}(\mathbf{w})$ satisfies:*

1. *L-smoothness: $\|\nabla\mathcal{L}(\mathbf{w}) - \nabla\mathcal{L}(\mathbf{w}')\| \leq L\|\mathbf{w} - \mathbf{w}'\|$*
2. *Polyak-Łojasiewicz condition: $\|\nabla\mathcal{L}(\mathbf{w})\|^2 \geq 2\mu(\mathcal{L}(\mathbf{w}) - \mathcal{L}^*)$ for some $\mu > 0$*

4.2 Main Convergence Result

We now formalize the convergence guarantees of the proposed continuous-time dynamics. The following theorem unifies both finite-time and fixed-time convergence regimes under a single parameterization.

Theorem 1. *Consider the continuous-time dynamics equation 5 with parameters satisfying $p_2 \in (0, 1)$, $p_1 < 2$, and $c_1, c_2 > 0$. Under Assumption 1: **(i) Finite-time convergence**: When $p_1 < 2$, there exists a finite time $T^* < \infty$ such that $\mathcal{L}(w(t)) = \mathcal{L}^*$ for all $t \geq T^*$. The convergence time is bounded by: $T^* \leq \frac{(\mathcal{L}(\mathbf{w}_0)-\mathcal{L}^*)^{1-\gamma_1}}{c_1 d^{-p_2}(2\mu)^{(1+p_2)/2}(1-\gamma_1)} + \frac{(\mathcal{L}(\mathbf{w}_0)-\mathcal{L}^*)^{1-\gamma_2}}{c_2 d^{p_1-2}(2\mu)^{(3-p_1)/2}(1-\gamma_2)}$ where $\gamma_1 = \frac{1+p_2}{2} \in (0.5, 1)$, $\gamma_2 = \frac{3-p_1}{2}$. **(ii) Fixed-time convergence**: When $p_1 < 1$, we have $\gamma_2 = \frac{3-p_1}{2} > 1$, and the convergence time is further bounded by a constant independent of initial conditions: $T^* \leq T_{\max} = \frac{1}{\alpha_2(\gamma_2-1)} + \frac{1}{\alpha_1(1-\gamma_1)}$, where $\alpha_1 = c_1 d^{-\frac{1-p_2}{2}}(2\mu)^{\frac{1+p_2}{2}}$ and $\alpha_2 = c_2 d^{p_1-2}(2\mu)^{\frac{3-p_1}{2}}$ are positive constants determined by problem parameters.*

Proof. The Proof details are shown in Appendix. C □

Remark 1. *The proof reveals distinct convergence phases depending on p_1: i)finite-time ($1 \leq p_1 < 2$): Both $\gamma_1, \gamma_2 < 1$, convergence time depends on initial conditions. (ii)Fixed-time ($p_1 < 1$): $\gamma_2 > 1$ dominates as $V(t) \to 0$, ensuring convergence time bounds independent of initial conditions This characterization highlights the practical flexibility of the dynamics: by tuning p_1, practitioners can trade off between rapid convergence with initial-condition dependence and guaranteed uniform convergence time.*

By using the explicit Euler discretization scheme, it yeilds:

$$\mathbf{w}_{k+1} = \mathbf{w}_k - \eta \left[c_1 \operatorname{sign}(\mathbf{g}_k) \odot |\mathbf{g}_k|^{p_2} + c_2 \operatorname{sign}(\mathbf{g}_k) \odot |\mathbf{g}_k|^{2-p_1}\right], \tag{6}$$

where η is the stepsize, and $\odot$ denotes element-wise multiplication. Therefore, the algorithm is shown in Algorithm 1.

Algorithm 1 Element-wise Finite/Fixed-Time (EFT) Convegence algorithm

Require: Parameters $\beta \in [0, 1)$, $c_1, c_2 > 0$, $p_1 < 2$, $p_2 \in (0, 1)$, learning rate $\eta > 0$.
Require: Initial weights $\mathbf{w}_0$,
1: **for** $k = 0, 1, 2, \ldots$ **do**
2: Compute gradients: $\mathbf{g}_k = \nabla\mathcal{L}(\mathbf{w}_k)$
3: Compute EFT forces: $F_k = c_1 \operatorname{sign}(\mathbf{g}_k) \odot |\mathbf{g}_k|^{p_2} + c_2 \operatorname{sign}(\mathbf{g}_k) \odot |\mathbf{g}_k|^{2-p_1}$
4: Update weights: $\mathbf{w}_{k+1} = \mathbf{w}_k - \eta F_k$
5: **end for**

4.3 Momentum-Enhanced Finite-Time Dynamics

Modern deep learning optimization faces two critical challenges: stochastic variance from mini-batch gradients and heterogeneous curvature across parameter space. We address these through two complementary momentum mechanisms that preserve our finite-time convergence guarantees while offering distinct computational advantages.

Element-wise Finite/Fixed-Time with Momentum (EFToM) For variance reduction in stochastic settings, we integrate exponential moving averages:

$$\mathbf{m}_k = \beta_1 \mathbf{m}_{k-1} + (1-\beta_1)\mathbf{g}_k, \tag{7a}$$

$$\mathbf{w}_{k+1} = \mathbf{w}_k - \eta \left[c_1 \operatorname{sign}(\mathbf{m}_k) \odot |\mathbf{m}_k|^{p_2} + c_2 \operatorname{sign}(\mathbf{m}_k) \odot |\mathbf{m}_k|^{2-p_1} \right]. \tag{7b}$$

where $\mathbf{m} \in \mathbb{R}^d$ is the momentum vector. The continuous-time analysis reveals that EFToM achieves momentum tracking through the system:

$$\dot{\mathbf{w}} = -c_1 \operatorname{sign}(\mathbf{m}) \odot |\mathbf{m}|^{p_2} - c_2 \operatorname{sign}(\mathbf{m}) \odot |\mathbf{m}|^{2-p_1}, \quad \dot{\mathbf{m}} = -\lambda (\mathbf{m} - \mathbf{g}), \tag{8a}$$

where $\lambda > 0$ controls the momentum convergence rate.

Element-wise Finite/Fixed-Time with Polyak Momentum (PEFToM) While EFToM excels in noisy environments, certain optimization landscapes benefit from accumulated gradient history. Polyak momentum provides this through its natural continuous representation. The discrete update $\mathbf{v}_k = \beta \mathbf{v}_{k-1} + \mathbf{g}_k$ can be unrolled as:

$$\mathbf{v}_k = \sum_{j=0}^{k} \beta^j \mathbf{g}_{k-j} = \mathbf{g}_k + \beta \mathbf{g}_{k-1} + \beta^2 \mathbf{g}_{k-2} + \dots \tag{9}$$

This discrete convolution has a natural continuous analog through the integral representation $\mathbf{v}(t) = \int_{-\infty}^{t} e^{-\gamma(t-s)} \mathbf{g}(s)\, ds$, where $\gamma > 0$ controls the memory depth. Taking the time derivative yields:

$$\frac{d\mathbf{v}}{dt} = \mathbf{g}(t) - \gamma \int_{-\infty}^{t} e^{-\gamma(t-s)} \mathbf{g}(s)\, ds = \mathbf{g}(t) - \gamma \mathbf{v}(t) \tag{10}$$

Unlike EFToM's instantaneous gradient tracking, PEFToM accumulates the complete gradient history, making it particularly effective for optimization problems with consistent gradient directions. The complete PEFToM system becomes:

$$\dot{\mathbf{v}} = \mathbf{g} - \gamma \mathbf{v}, \quad \dot{\mathbf{w}} = -c_1 \operatorname{sign}(\mathbf{v}) \odot |\mathbf{v}|^{p_2} - c_2 \operatorname{sign}(\mathbf{v}) \odot |\mathbf{v}|^{2-p_1}. \tag{11a}$$

Theorem 2 (EFToM Finite-/Fixed-Time Convergence)**.** *Consider the EFToM dynamics equation 8 with parameters $p_2 \in (0,1)$, $0 < p_1 < 2$, and $c_1, c_2, \lambda > 0$. Under Assumption 1, choose $\lambda \geq \lambda_\star$, where $\lambda_\star := \max\left\{ \left(\frac{4K_1}{c_1}\right)^{1-\theta_1}, \left(\frac{4K_2}{c_2}\right)^{1-\theta_2} \right\}$ with $\theta_1 = \frac{2p_2}{1+p_2}$, $\theta_2 = \frac{2(2-p_1)}{3-p_1}$. Define the exponents $\alpha := \frac{1+p_2}{2} \in (\frac{1}{2}, 1)$, $\beta := \frac{3-p_1}{2}$, and constants $\hat{a} := \frac{1}{2} c_1 d^{-\frac{1-p_2}{2}} (2\mu)^\alpha$, $\hat{b} := \frac{1}{2} c_2 d^{-\frac{1-p_1}{2}} (2\mu)^\beta$. Then the following convergence guarantees hold:* ***(i) Finite-time convergence*** *($1 \leq p_1 < 2$, equivalently $\beta \leq 1$): For any initial state $(\mathbf{w}(0), \mathbf{m}(0))$, the convergence time satisfies $T \leq \frac{V_{tot}(0)^{1-\alpha}}{\hat{a}(1-\alpha)} + \frac{V_{tot}(0)^{1-\beta}}{\hat{b}(1-\beta)}$, where $V_{tot}(0) := \mathcal{L}(\mathbf{w}(0)) - \mathcal{L}^* + \frac{c_1}{2}\|\mathbf{m}(0) - \mathbf{g}(0)\|^2$.* ***(ii) Fixed-time convergence*** *If $p_1 < 1$, every trajectory reaches the global optimum $(\mathbf{w}^*, \mathbf{0})$ within time $T_{\max} = \frac{1}{\hat{a}(1-\alpha)} + \frac{1}{\hat{b}(\beta-1)}$.*

Proof. The Proof details are shown in Appendix D □

Theorem 3 (PEFToM Finite-/Fixed-Time Convergence)**.** *Consider the PEFToM dynamics equation 11 with the same parameter conditions as Theorem 2. Under Assumption 1, the convergence guarantees are analogous to EFToM, with constants: $\hat{a} := \frac{\gamma}{2} c_1 d^{-\frac{1-p_2}{2}} (2\mu)^\alpha$, $\hat{b} := \frac{\gamma}{2} c_2 d^{-\frac{1-p_1}{2}} (2\mu)^\beta$.*

Proof. See Appendix E for the complete proof. □

Remark 2 (Momentum Mechanism Selection Guide)**.** *The theoretical analysis reveals distinct algorithmic characteristics: (i) EFToM: Convergence rates independent of momentum parameter λ, providing robustness to hyperparameter selection. The parameter λ only affects the admissibility threshold $\lambda_\star$, making hyperparameter tuning less critical. (ii) PEFToM: Convergence constants*

scale linearly with damping parameter γ, offering direct control over convergence acceleration. However, this requires careful γ selection to balance convergence speed with numerical stability. The fundamental difference lies in parameter sensitivity: EFToM prioritizes robustness through parameter-independent convergence rates, while PEFToM enables fine-tuned acceleration through direct parameter control over convergence constants.

Discretizing equation 11 using explicit Euler methods, it yields

$$\mathbf{w}_{k+1} = \mathbf{w}_k - \eta \left(c_1 \operatorname{sign}(\mathbf{v}_k) \odot |\mathbf{v}_k|^{p_2} + c_2 \operatorname{sign}(\mathbf{v}_k) \odot |\mathbf{v}_k|^{2-p_1} \right), \tag{12a}$$

$$\mathbf{v}_{k+1} = \beta \, \mathbf{v}_k + \mathbf{g}_k, \tag{12b}$$

Based on (7) and (12), the EFToM and PEFToM are sumarized in Algorithm 2 and 3, respectively.

Algorithm 2 Element-wise Finite-Time with Momentum (EFToM)

Require: Parameters $\beta \in [0, 1)$, $c_1, c_2 \geq 0$, $p_1 < 2$, $p_2 \in (0, 1)$, learning rate $\eta > 0$
Require: Initial weights $\mathbf{w}0$, initial momentum $v_0 = 0$
for $k = 0, 1, 2, \ldots$ **do**
  $\mathbf{g}_k = \nabla \mathcal{L}(\mathbf{w}_k)$
  $\mathbf{m}_{k+1} = \beta \mathbf{m}_k + (1 - \beta)\mathbf{g}_k$.
  $F_k = c_1 \operatorname{sign}(\mathbf{m}_k) \odot |\mathbf{m}_k|^{p_2} + c_2 \operatorname{sign}(\mathbf{m}_k) \odot |\mathbf{m}_k|^{2-p_1}$
  Update weights: $\mathbf{w}_{k+1} = \mathbf{w}_k - \eta F_k$
end for

Algorithm 3 Element-wise Finite-Time with Polyak Momentum (PEFToM)

Require: Parameters $\beta \in [0, 1)$, $c_1, c_2 \geq 0$, $p_1 < 2$, $p_2 \in (0, 1)$, learning rate $\eta > 0$
Require: Initial weights $\mathbf{w}0$, initial momentum $v_0 = 0$
for $k = 0, 1, 2, \ldots$ **do**
  $\mathbf{g}_k = \nabla \mathcal{L}(\mathbf{w_k})$
  $\mathbf{v}_{k+1} = \beta \mathbf{v}_k + \mathbf{g}_k$.
  $F_k = c_1 \operatorname{sign}(\mathbf{v}_k) \odot |\mathbf{v}_k|^{p_2} + c_2 \operatorname{sign}(\mathbf{v}_k) \odot |\mathbf{v}_k|^{2-p_1}$
  Update weights: $\mathbf{w}_{k+1} = \mathbf{w}_k - \eta F_k$
end for

4.4 Unified Framework: SignSGD and Signum as Special Cases

Our element-wise finite-time framework provides a unified theoretical foundation for sign-based optimization methods. For instance, SignSGD corresponds to the limiting behavior when $p_1 \to 2$ and $p_2 \to 0$ in our EFT dynamics :$\lim_{p_1 \to 2, p_2 \to 0} \dot{\mathbf{w}} = -(c_1 + c_2)\text{sign}(\mathbf{g})$. Under Euler discretization with step size η, this yields: $\mathbf{w}_{k+1} = \mathbf{w}_k - \eta(c_1 + c_2)\text{sign}(\mathbf{g}_k)$. Similarly, Signum (Bernstein et al., 2018) emerges from our EFToM under the same parameter limits. When $p_1 \to 2$ and $p_2 \to 0$:

$$\mathbf{m}_k = \beta_1 \mathbf{m}_{k-1} + (1 - \beta_1)\mathbf{g}_k, \qquad \mathbf{w}_{k+1} = \mathbf{w}_k - \eta(c_1 + c_2)\text{sign}(\mathbf{m}_k). \tag{13}$$

5 Numerical Experiments

We empirically validate the proposed Element-wise Finite-Time Optimization (EFT) framework, including its variants EFToM and PEFToM, on standard benchmarks across two domains. For computer vision, we evaluate performance on image classification tasks with CIFAR-10 and CIFAR-100 (Krizhevsky, 2009) . For natural language processing task, we pretrain the llama-60m on C4 (Muennighoff et al., 2023) subset. We compare our methods against a comprehensive suite of optimization baselines to demonstrate their effectiveness. All experiments are implemented in PyTorch and executed on a single NVIDIA RTX 4090 GPU with 24 GB memory.

5.1 Image Classification on CIFAR Datasets

Setup We evaluate on CIFAR-10 and CIFAR-100 using three CNN architectures: VGG-11, ResNet-34, and DenseNet-121. Training proceeds for 200 epochs with batch size 128, learning rate decay (×0.1 at epoch 150), and weight decay 5×10^{-4}. Baseline optimizers include SGD, SGD with momentum (SGDM), AdamW, AdaBelief, SignSGD, Signum, Lion, and FxTS-GF(M). For hyperparameters, we follow the setting in Zhuang et al. (2020), with details of the hyperparameters used in the experiment given in Appendix F.

Table 1: Test accuracy (%) on CIFAR-10 & CIFAR-100 at different epochs and architectures.

	CIFAR10			CIFAR100		
	VGG-11	ResNet-34	DenseNet-121	VGG-11	ResNet-34	DenseNet-121
Epochs	200	200	200	200	200	200
SGD	86.97	92.69	91.77	62.86	75.95	77.92
SignSGD	48.13	92.86	92.9	29.59	67.38	68.88
EFT	88.78	94	94.33	64.0	75.74	77.72
FxTS-GF(M)	87.91	93.44	94.58	63.67	73.58	74.65
EFToM	89.01	94.33	94.64	65.39	75.78	77.31
Signum	88.04	94.19	94.64	58.53	73.51	75.43
Lion	87.02	94.25	94.44	57.21	72.99	75.23
AdamW	87.97	93.88	94.07	58.66	71.98	75.16
AdaBelief	87.86	94.26	94.06	58.37	72.08	74.01
SGDM	90.35	94.68	94.8	64.62	75.82	78.1
PEFToM	**91.02**	**95.17**	**95.62**	**68.05**	**77.34**	**79.6**

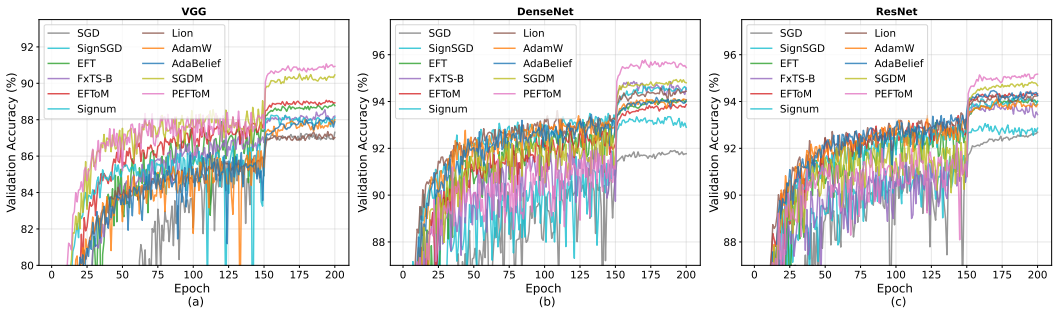

Figure 2: Test accuracy for CIFAR10 with different optimizers and models: (a) VGG-11, (b) DenseNet-121, (c) ResNet-34

.

Performance Analysis Table 1 presents final accuracies across architectures and datasets, while Figure 2 and Figure 5.1 present the test accuracy of various optimizers at different training stage. The proposed framework achieves consistent improvements, with PEFToM reaching 95.17% on CIFAR-10 ResNet-34 and 79.6% on CIFAR-100 DenseNet-121. These results represent gains of +0.49% and +1.5% over SGD with momentum. The progression from EFT $\rightarrow$ EFToM $\rightarrow$ PEFToM demonstrates systematic enhancement through momentum integration. On CIFAR-100 ResNet-34: EFT (75.74%) $\rightarrow$ EFToM (75.78%) $\rightarrow$ PEFToM (77.34%) shows incremental but meaningful improvements from each algorithmic component. Performance advantages become more pronounced on the challenging CIFAR-100 dataset. PEFToM surpasses modern adaptive methods: +5.36% over AdamW (77.34% vs 71.98%) and +5.26% over AdaBelief (77.34% vs 72.08%) on ResNet-34. This pattern suggests finite-time optimization principles provide greater benefits as task complexity increases. Our element-wise approach addresses instabilities observed in existing sign-based methods. While SignSGD deteriorates significantly on CIFAR-100 (29.59% on VGG-11), EFToM maintains robust performance across all configurations. Similarly, compared to FxTS-GF(M) which suffers from dimensional coupling, our method shows superior consistency on CIFAR-100 ResNet-34.

5.2 Language Model Pretraining

We pretrain Llama-60M on C4 subset (Muennighoff et al., 2023) for 30,000 steps with batch size 16. Table 2 reports training and validation losses at key checkpoints, and the traning loss curve are demonstrated in Figure 4. EFToM achieves the lowest validation loss (3.929 at 30k steps), outperforming AdamW (4.045) and other baselines. The rapid convergence aligns with our finite-time optimization theory. While AdamW exhibits smoother training curves, EFToM reaches better final performance despite some oscillation. PEFToM shows different behavior with slower initial progress but competitive endpoints (4.594), indicating momentum variants may suit different training phases. The language modeling results validate our framework's applicability beyond computer vision. EFToM's validation performance significantly exceeds AdamW (+2.9% relative improve-

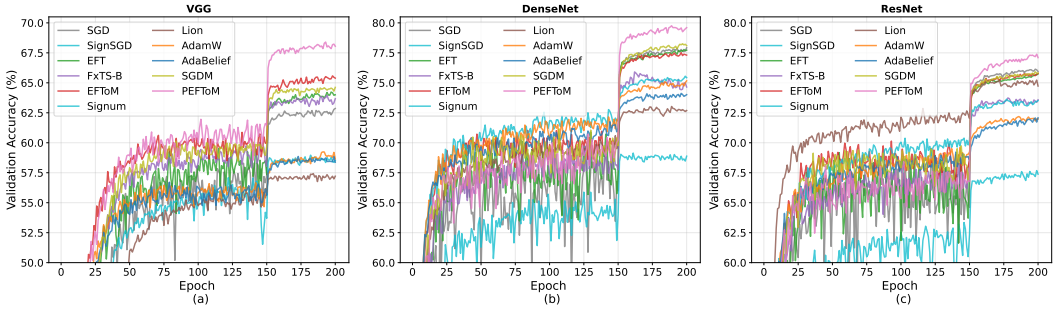

Figure 3: Test accuracy for CIFAR100 with different optimizers and models: (a) VGG-11, (b) DenseNet-121, (c) ResNet-34

.

ment) and AdaBelief (+5.5% relative improvement), demonstrating effectiveness for large-scale sequence modeling.

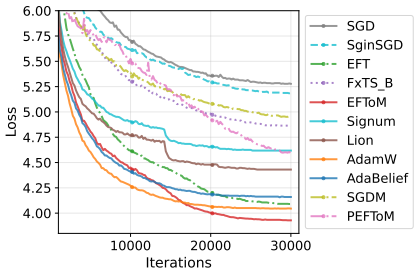

Figure 4: Test loss on C4 dataset

Table 2: Train and validation loss on C4 at different iterations.

	Train Loss				Test Loss			
Optimizer	5k	10k	20k	30k	5k	10k	20k	30k
SGD	5.875	5.938	5.469	5.219	6.125	5.708	5.354	5.278
SignSGD	5.625	5.875	5.406	5.904	5.903	5.615	5.292	5.188
EFT	5.000	4.875	4.500	4.125	5.177	4.618	4.208	4.090
FxTS-GF(M)	5.531	5.594	5.188	4.844	5.729	5.319	4.983	4.858
EFToM	4.688	4.688	**4.344**	**3.953**	4.806	4.451	**4.003**	**3.929**
Signum	4.969	5.156	4.875	4.563	5.153	4.910	4.660	4.618
Lion	4.875	5.031	4.719	4.438	5.003	4.764	4.479	4.431
AdamW	**4.531**	**4.500**	4.406	4.031	**4.604**	**4.2708**	4.066	4.045
AdaBelief	4.656	4.656	4.500	4.156	4.764	4.410	4.186	4.160
SGDM	5.469	5.594	5.188	4.844	5.705	5.389	5.076	4.951
PEFToM	5.563	5.781	5.125	4.625	5.809	5.524	4.934	4.594

5.3 Discussion

Our element-wise finite-time dynamics consistently improve performance across diverse architectures while successfully integrating momentum mechanisms that preserve theoretical convergence properties. *Memory Efficiency*: Our methods reduce memory overhead by approximately 33% compared to Adam-family optimizers by requiring only first-order momentum buffers, making them suitable for large-scale model training. *Momentum Selection*: PEFToM excels on vision tasks while EFToM performs best for language modeling, indicating that momentum mechanism selection should consider task-specific optimization characteristics.

6 Conclusion

We developed an element-wise finite-time optimization framework that addresses the scalability limitations of control-theoretic methods in high-dimensional deep learning. By eliminating dimensional coupling through coordinate-independent dynamics, our approach achieves rigorous finite/fixed-time convergence guarantees while preserving the heterogeneity-aware adaptivity crucial for neural network optimization. The theoretical framework unifies disparate optimization methods under a principled foundation: SignSGD and Signum emerge as limiting cases, providing rigorous finite-time theoretical justification for their empirical success. Our momentum-enhanced variants demonstrate that classical acceleration techniques can be seamlessly integrated without compromising convergence properties. Empirical validation across computer vision and language modeling confirms both convergence acceleration and memory efficiency gains, positioning our methods as theoretically grounded yet practically viable alternatives to adaptive optimizers. This work establishes a new paradigm connecting control-theoretic stability with large-scale machine learning.

Reproducibility Statement

To ensure reproducibility, we provide complete implementation details in Appendix F, theoretical proofs in Appendices C–E, and experimental configurations in Section 5. All datasets used (CIFAR-10/100, C4) are publicly available as described in Section 5. We will release the complete source code upon acceptance of this paper.

References

Kang An, Yuxing Liu, Rui Pan, Shiqian Ma, Donald Goldfarb, and Tong Zhang. Asgo: Adaptive structured gradient optimization, 2025. URL https://arxiv.org/abs/2503.20762.

Jeremy Bernstein, Yu-Xiang Wang, Kamyar Azizzadenesheli, and Animashree Anandkumar. signSGD: Compressed optimisation for non-convex problems. In Jennifer Dy and Andreas Krause (eds.), *Proceedings of the 35th International Conference on Machine Learning*, volume 80 of *Proceedings of Machine Learning Research*, pp. 560–569. PMLR, 10–15 Jul 2018. URL https://proceedings.mlr.press/v80/bernstein18a.html.

Sanjay P Bhat and Dennis S Bernstein. Finite-time stability of continuous autonomous systems. *SIAM Journal on Control and optimization*, 38(3):751–766, 2000.

Param Budhraja, Mayank Baranwal, Kunal Garg, and Ashish Hota. Breaking the convergence barrier: Optimization via fixed-time convergent flows. In *Proceedings of the AAAI Conference on Artificial Intelligence*, volume 36, pp. 6115–6122, 2022.

Gang Chen and Zhiyong Li. A fixed-time convergent algorithm for distributed convex optimization in multi-agent systems. *Automatica*, 95:539–543, 2018. ISSN 0005-1098. doi: https://doi.org/10.1016/j.automatica.2018.05.032. URL https://www.sciencedirect.com/science/article/pii/S0005109818302747.

Xiangning Chen, Chen Liang, Da Huang, Esteban Real, Kaiyuan Wang, Hieu Pham, Xuanyi Dong, Thang Luong, Cho-Jui Hsieh, Yifeng Lu, et al. Symbolic discovery of optimization algorithms. *Advances in neural information processing systems*, 36:49205–49233, 2023.

Zhaorui Dong, Yushun Zhang, Zhi-Quan Luo, Jianfeng Yao, and Ruoyu Sun. Towards quantifying the hessian structure of neural networks, 2025. URL https://arxiv.org/abs/2505.02809.

John C. Duchi, Elad Hazan, and Yoram Singer. Adaptive subgradient methods for online learning and stochastic optimization. *J. Mach. Learn. Res.*, 12:2121–2159, 2011.

Kunal Garg and Dimitra Panagou. Fixed-time stable gradient flows: Applications to continuous-time optimization. *IEEE Transactions on Automatic Control*, 66(5):2002–2015, 2021. doi: 10.1109/TAC.2020.3001436.

Vineet Gupta, Tomer Koren, and Yoram Singer. Shampoo: Preconditioned stochastic tensor optimization. In *International Conference on Machine Learning*, 2018.

Godfrey Harold Hardy, John Edensor Littlewood, and George Pólya. *Inequalities*. Cambridge university press, 1952.

Hassan K Khalil and Jessy W Grizzle. *Nonlinear systems*, volume 3. Prentice hall Upper Saddle River, NJ, 2002.

Diederik P Kingma and Jimmy Ba. Adam: A method for stochastic optimization. *arXiv preprint arXiv:1412.6980*, 2014.

Alex Krizhevsky. Learning multiple layers of features from tiny images. *MSc thesis*, 2009.

Hong Liu, Zhiyuan Li, David Hall, Percy Liang, and Tengyu Ma. Sophia: A scalable stochastic second-order optimizer for language model pre-training. *arXiv preprint arXiv:2305.14342*, 2023.

Yang Liu, Hongyi Li, Renquan Lu, Zongyu Zuo, and Xiaodi Li. An overview of finite/fixed-time control and its application in engineering systems. *IEEE/CAA Journal of Automatica Sinica*, 9 (12):2106–2120, 2022.

Ilya Loshchilov and Frank Hutter. Decoupled weight decay regularization. *arXiv preprint arXiv:1711.05101*, 2017.

Niklas Muennighoff, Alexander M Rush, Boaz Barak, Teven Le Scao, Aleksandra Piktus, Nouamane Tazi, Sampo Pyysalo, Thomas Wolf, and Colin Raffel. Scaling data-constrained language models. *arXiv preprint arXiv:2305.16264*, 2023.

Yurii Nesterov. A method for solving the convex programming problem with convergence rate o(1/k^2). *Proceedings of the USSR Academy of Sciences*, $269 : 543 - -547, 1983. URL$.

Lien T Nguyen, Xinghuo Yu, Andrew Eberhard, and Chaojie Li. Fixed-time gradient dynamics with time-varying coefficients for continuous-time optimization. *IEEE Transactions on Automatic Control*, 68(7):4383–4390, 2022.

Antonio Orvieto and Robert Gower. In search of adam's secret sauce. *arXiv preprint arXiv:2505.21829*, 2025.

B.T. Polyak. Some methods of speeding up the convergence of iteration methods. *USSR Computational Mathematics and Mathematical Physics*, 4(5):1–17, 1964. ISSN 0041-5553. https://doi.org/10.1016/0041-5553(64)90137-5. URL https://www.sciencedirect.com/science/article/pii/0041555364901375.

Andrey Polyakov. Nonlinear feedback design for fixed-time stabilization of linear control systems. *IEEE transactions on Automatic Control*, 57(8):2106–2110, 2011.

Nikhil Vyas, Depen Morwani, Rosie Zhao, Mujin Kwun, Itai Shapira, David Brandfonbrener, Lucas Janson, and Sham Kakade. Soap: Improving and stabilizing shampoo using adam. *arXiv preprint arXiv:2409.11321*, 2024.

Yang You, Jing Li, Sashank Reddi, Jonathan Hseu, Sanjiv Kumar, Srinadh Bhojanapalli, Xiaodan Song, James Demmel, Kurt Keutzer, and Cho-Jui Hsieh. Large batch optimization for deep learning: Training bert in 76 minutes. *arXiv preprint arXiv:1904.00962*, 2019.

Yushun Zhang, Congliang Chen, Tian Ding, Ziniu Li, Ruoyu Sun, and Zhi-Quan Luo. Why transformers need adam: A hessian perspective. In A. Globerson, L. Mackey, D. Belgrave, A. Fan, U. Paquet, J. Tomczak, and C. Zhang (eds.), *Advances in Neural Information Processing Systems*, volume 37, pp. 131786–131823. Curran Associates, Inc., 2024a. URL https://proceedings.neurips.cc/paper_files/paper/2024/file/ee0e45ff4de76cbfdf07015a7839f339-Paper-Conference.pdf.

Yushun Zhang, Congliang Chen, Ziniu Li, Tian Ding, Chenwei Wu, Diederik P Kingma, Yinyu Ye, Zhi-Quan Luo, and Ruoyu Sun. Adam-mini: Use fewer learning rates to gain more. *arXiv preprint arXiv:2406.16793*, 2024b.

Juntang Zhuang, Tommy Tang, Yifan Ding, Sekhar C Tatikonda, Nicha Dvornek, Xenophon Papademetris, and James Duncan. Adabelief optimizer: Adapting stepsizes by the belief in observed gradients. *Advances in neural information processing systems*, 33:18795–18806, 2020.

A LARGE LANGUAGE MODEL USAGE STATEMENT

Large Language Models (LLMs) were used in this research for the following purposes: (i) **Writing assistance:** LLMs were used to aid in polishing the manuscript, including grammar checking, sentence structure improvement, and clarity enhancement of technical explanations. (ii)**Literature review support:** LLMs assisted in discovering and organizing related work during the literature review process, helping to identify relevant papers and research directions in optimization theory and deep learning. All substantial intellectual contributions, including the element-wise finite-time optimization framework, experimental design, and analysis of results, were developed independently by the authors.

B FOUNDATIONS OF FINITE-TIME AND FIXED-TIME STABILITY THEORY

This appendix provides a comprehensive foundation for finite-time and fixed-time stability theory, establishing the mathematical framework underlying our element-wise optimization methods. We present detailed proofs of the fundamental lemmas and establish all necessary mathematical tools used throughout the paper.

B.1 NOTATION AND PRELIMINARY DEFINITIONS

Throughout this appendix, we consider autonomous dynamical systems of the form:

$$\dot{\mathbf{x}}(t) = f(\mathbf{x}(t)), \quad \mathbf{x}(0) = \mathbf{x}_0 \in \mathbb{R}^n \tag{14}$$

where $f : \mathbb{R}^n \to \mathbb{R}^n$ is locally Lipschitz continuous, and $\mathbf{x} = \mathbf{0}$ is an equilibrium point (i.e., $f(\mathbf{0}) = \mathbf{0}$).

Notation $\|\cdot\|$ is Euclidean norm in $\mathbb{R}^n$, $\mathcal{B}_r := \{\mathbf{x} \in \mathbb{R}^n : \|\mathbf{x}\| \leq r\}$ represents closed ball of radius r, $\mathcal{B}_r^o := \{\mathbf{x} \in \mathbb{R}^n : \|\mathbf{x}\| < r\}$ represents open ball of radius r, $V : \mathbb{R}^n \to \mathbb{R}_+$ is the Lyapunov function candidate, $\dot{V}(\mathbf{x}) := \nabla V(\mathbf{x})^T f(\mathbf{x})$ represents time derivative of V along system trajectories, $\mathbb{R}_+ := [0, +\infty)$ is non-negative real numbers.

B.2 CLASSICAL ASYMPTOTIC STABILITY VS. FINITE-TIME CONVERGENCE

Definition 3 (Asymptotic Stability Khalil & Grizzle (2002))**.** *The equilibrium $\mathbf{x} = \mathbf{0}$ is asymptotically stable if:*

1. ***Stability**: For any $\epsilon > 0$, there exists $\delta > 0$ such that $\|\mathbf{x}_0\| < \delta$ implies $\|\mathbf{x}(t)\| < \epsilon$ for all $t \geq 0$*
2. ***Attractivity**: There exists $\delta > 0$ such that $\|\mathbf{x}_0\| < \delta$ implies $\lim_{t\to\infty} \mathbf{x}(t) = \mathbf{0}$*

The fundamental limitation of asymptotic stability is that convergence occurs only as $t \to \infty$. In contrast, finite-time stability guarantees exact convergence in finite time, providing stronger convergence guarantees essential for time-critical applications.

B.3 FINITE-TIME STABILITY THEORY

Definition 4 (Finite-Time Stability Bhat & Bernstein (2000))**.** *The equilibrium $\mathbf{x} = \mathbf{0}$ is finite-time stable if:*

1. *It is asymptotically stable*
2. *For any initial condition $\mathbf{x}_0$ in a neighborhood of the origin, there exists a settling time $T(\mathbf{x}_0) < \infty$ such that $\mathbf{x}(t) = \mathbf{0}$ for all $t \geq T(\mathbf{x}_0)$*

*The function $T : \mathcal{B}_r^o \to \mathbb{R}_+$ is called the **settling time function**.*

B.3.1 Fundamental Lemma for Finite-Time Convergence

Lemma 3 (Finite-Time Convergence via Fractional Powers Bhat & Bernstein (2000)). *Let $V(t) \geq 0$ be an absolutely continuous function satisfying the differential inequality:*

$$\dot{V}(t) \leq -\alpha V(t)^{\gamma}. \tag{15}$$

for some constants $\alpha > 0$ and $\gamma \in (0, 1)$. Then $V(t)$ reaches zero in finite time $T^* < \infty$ given by:

$$T^* \leq \frac{V(0)^{1-\gamma}}{\alpha(1-\gamma)}. \tag{16}$$

Proof. We establish this result through direct integration using separation of variables. The differential inequality equation 15 gives us:

$$\frac{dV}{dt} \leq -\alpha V^{\gamma}. \tag{17}$$

For $V(t) > 0$ (which holds for $t < T^*$), we can separate variables:

$$\frac{dV}{V^{\gamma}} \leq -\alpha dt. \tag{18}$$

Integrating both sides from 0 to t (where $t < T^*$):

$$\int_{V(0)}^{V(t)} V^{-\gamma} dV \leq -\alpha \int_0^t ds = -\alpha t. \tag{19}$$

The left-hand side evaluates to:

$$\int_{V(0)}^{V(t)} V^{-\gamma} dV = \left[\frac{V^{1-\gamma}}{1-\gamma}\right]_{V(0)}^{V(t)} = \frac{V(t)^{1-\gamma} - V(0)^{1-\gamma}}{1-\gamma}. \tag{20}$$

Since $\gamma \in (0, 1)$, we have $1 - \gamma > 0$, thus:

$$\frac{V(t)^{1-\gamma} - V(0)^{1-\gamma}}{1-\gamma} \leq -\alpha t. \tag{21}$$

Rearranging:

$$V(t)^{1-\gamma} \leq V(0)^{1-\gamma} - \alpha(1-\gamma)t. \tag{22}$$

The right-hand side becomes zero when:$t = T^* := \frac{V(0)^{1-\gamma}}{\alpha(1-\gamma)}$. For $t \geq T^*$, we must have $V(t) = 0$ (since $V(t) \geq 0$ by assumption), establishing finite-time convergence. □

Remark 3. *The crucial insight is that the fractional power $\gamma < 1$ creates a "super-linear" decay rate near the equilibrium. As $V(t) \to 0$, the term $V(t)^{\gamma}$ decays more slowly than $V(t)$, leading to finite-time convergence rather than asymptotic approach.*

B.4 Fixed-Time Stability Theory

The limitation of finite-time stability is that the settling time $T(\mathbf{x}_0)$ may grow unboundedly as $\|\mathbf{x}_0\| \to \infty$. Fixed-time stability addresses this by providing uniform bounds independent of initial conditions.

Definition 5 (Fixed-Time Stability Polyakov (2011)). *A finite-time stable equilibrium $\mathbf{x} = \mathbf{0}$ is called fixed-time stable if the settling time function $T(\mathbf{x}_0)$ is globally bounded:* $\sup_{\mathbf{x}_0 \in \mathbb{R}^n} T(\mathbf{x}_0) < \infty$.

B.4.1 DUAL-POWER LEMMA FOR FIXED-TIME CONVERGENCE

Lemma 4 (Fixed-Time Convergence via Dual Powers Polyakov (2011)). *Let $V(t) \geq 0$ be an absolutely continuous function satisfying:*

$$\dot{V}(t) \leq -aV(t)^{\alpha} - bV(t)^{\beta} \tag{23}$$

for constants $a, b > 0$, $0 < \alpha < 1 < \beta$. Then $V(t)$ reaches zero in fixed time bounded by:

$$T_{\max} = \frac{1}{a(1-\alpha)} + \frac{1}{b(\beta-1)}. \tag{24}$$

Proof. We analyze the convergence behavior in two distinct phases based on the magnitude of $V(t)$.

Phase 1 ($V(t) \geq 1$): When $V(t) \geq 1$, since $\beta > \alpha$, we have $V(t)^{\beta} \geq V(t)^{\alpha}$. The differential inequality equation 23 becomes:

$$\dot{V} \leq -aV^{\alpha} - bV^{\beta} \leq -(a+b)V^{\beta}. \tag{25}$$

Applying the separation of variables technique:

$$\frac{dV}{V^{\beta}} \leq -(a+b)dt. \tag{26}$$

Integrating from $V(0)$ to 1 (assuming $V(0) > 1$):

$$\int_{V(0)}^{1} V^{-\beta} dV \leq -(a+b)T_1. \tag{27}$$

Evaluating the integral:

$$\left[\frac{V^{1-\beta}}{1-\beta}\right]_{V(0)}^{1} = \frac{1 - V(0)^{1-\beta}}{1-\beta} \leq -(a+b)T_1. \tag{28}$$

Since $\beta > 1$, we have $1 - \beta < 0$, therefore:

$$\frac{V(0)^{1-\beta} - 1}{\beta - 1} \leq (a+b)T_1. \tag{29}$$

This gives us:

$$T_1 \leq \frac{V(0)^{1-\beta} - 1}{(a+b)(\beta-1)} \leq \frac{1}{b(\beta-1)}. \tag{30}$$

Phase 2 ($V(t) \leq 1$): When $V(t) \leq 1$, since $\alpha < 1$, we have $V(t)^{\alpha} \geq V(t)^{\beta}$. The differential inequality becomes:

$$\dot{V} \leq -aV^{\alpha} - bV^{\beta} \leq -(a+b)V^{\alpha}. \tag{31}$$

Following similar integration:

$$T_2 \leq \frac{1^{1-\alpha}}{(a+b)(1-\alpha)} = \frac{1}{a(1-\alpha)}. \tag{32}$$

Total convergence time: The total time to reach $V(t) = 0$ is:

$$T_{\max} = T_1 + T_2 \leq \frac{1}{b(\beta-1)} + \frac{1}{a(1-\alpha)}. \tag{33}$$

Importantly, this bound is independent of the initial condition $V(0)$. □

Remark 4. *The dual-power structure in equation 23 ensures optimal convergence characteristics:*

- *For large $V(t)$: the V^{β} term (with $\beta > 1$) dominates, providing rapid initial convergence*
- *For small $V(t)$: the V^{α} term (with $\alpha < 1$) dominates, ensuring finite-time convergence to zero*

This mechanism guarantees both fast convergence and uniform settling time bounds.

B.5 Essential Mathematical Tools

This section establishes the key mathematical inequalities and lemmas used throughout our proofs.

Lemma 5 (Young's Inequality (Hardy et al., 1952, Chap. I)). *Let $a, b \geq 0$ and let $p, q > 1$ be Hölder conjugates, i.e. $\frac{1}{p} + \frac{1}{q} = 1$. Then $ab \leq \frac{a^p}{p} + \frac{b^q}{q}$. More generally, for any $\varepsilon > 0$ one has $ab \leq \frac{\varepsilon^p}{p} a^p + \frac{\varepsilon^{-q}}{q} b^q$, which is often used to split mixed terms into pure powers.*

Lemma 6 (Hardy et al. (1952)). *For any $x_1, \ldots, x_m \in \mathbb{R}$ and $q > 0$:*

1. *If $0 < q \leq 1$: $(\sum_{i=1}^m |x_i|)^q \leq \sum_{i=1}^m |x_i|^q$*
2. *If $q > 1$: $(\sum_{i=1}^m |x_i|)^q \leq m^{q-1} \sum_{i=1}^m |x_i|^q$*

Throughout the appendix every vector operation ($|\cdot|^q$, *sign*, $\odot$) is taken *element-wise*.

C Corrected Proof of Element-wise Finite-Time Convergence

C.1 Main Theorem

Proof. Recall the element-wise dynamics:

$$\dot{\mathbf{w}} = -c_1 \operatorname{sign}(\mathbf{g}) \odot |\mathbf{g}|^{p_2} - c_2 \operatorname{sign}(\mathbf{g}) \odot |\mathbf{g}|^{2-p_1} \tag{34}$$

where $c_1, c_2 > 0$, $p_2 \in (0,1)$, $p_1 \in (0,3)$, and $\mathbf{g} = \nabla \mathcal{L}(\mathbf{w})$. Consider the Lyapunov function $V(t) = \mathcal{L}(\mathbf{w}(t)) - \mathcal{L}^*$, it yeilds:

$$\dot{V}(t) = \sum_{i=1}^d g_i \dot{w}_i = -c_1 \sum_{i=1}^d g_i \cdot \operatorname{sign}(g_i) |g_i|^{p_2} - c_2 \sum_{i=1}^d g_i \cdot \operatorname{sign}(g_i) |g_i|^{2-p_1} \tag{35}$$

$$= -c_1 \sum_{i=1}^d |g_i|^{1+p_2} - c_2 \sum_{i=1}^d |g_i|^{3-p_1}. \tag{36}$$

First, we bound $\sum_{i=1}^d |g_i|^{1+p_2}$. Since $p_2 \in (0,1)$, we have $1 + p_2 \in (1,2)$. Applying Lemma 6 with $q = 1 + p_2 > 1$:

$$\left(\sum_{i=1}^d |g_i| \right)^{1+p_2} \leq d^{p_2} \sum_{i=1}^d |g_i|^{1+p_2}. \tag{37}$$

Rearranging:

$$\sum_{i=1}^d |g_i|^{1+p_2} \geq d^{-p_2} \left(\sum_{i=1}^d |g_i| \right)^{1+p_2}. \tag{38}$$

Next, we bound $\sum_{i=1}^d |g_i|^{3-p_1}$. Since $p_1 < 2$, then $3 - p_1 > 1$. Using Lemma 6 with $q > 1$:

$$\sum_{i=1}^d |g_i|^{3-p_1} \geq d^{-(3-p_1-1)} \left(\sum_{i=1}^d |g_i| \right)^{3-p_1} = d^{p_1-2} \left(\sum_{i=1}^d |g_i| \right)^{3-p_1}. \tag{39}$$

Using the fundamental inequality $\sum_{i=1}^d |g_i| \geq \|\mathbf{g}\|_2$ and the PL condition $\|\mathbf{g}\|_2^2 \geq 2\mu V$:

$$\sum_{i=1}^d |g_i| \geq \|\mathbf{g}\|_2 \geq \sqrt{2\mu V}. \tag{40}$$

Combining the above results, it yeilds:

$$\dot{V}(t) \leq -c_1 d^{-p_2} (2\mu V)^{(1+p_2)/2} - c_2 d^{p_1-2} (2\mu V)^{(3-p_1)/2}, \tag{41}$$

Define: $\alpha_1 := c_1 d^{-p_2}(2\mu)^{(1+p_2)/2} > 0$, $\alpha_2 := c_2 d^{p_1-2}(2\mu)^{(3-p_1)/2} > 0$, $\gamma_1 := \frac{1+p_2}{2} \in \left(\frac{1}{2}, 1\right)$, $\gamma_2 := \frac{3-p_1}{2}$, it yields:

$$\dot{V}(t) \leq -\alpha_1 V^{\gamma_1} - \alpha_2 V^{\gamma_2}. \tag{42}$$

Finite-time convergence: Since $\gamma_1 < 1$, by finite-time stability theory (Lemma 3), the system converges in finite time with settling time bound:

$$T \leq \frac{V(0)^{1-\gamma_1}}{\alpha_1(1-\gamma_1)} + \frac{V(0)^{1-\gamma_2}}{\alpha_2(1-\gamma_2)}. \tag{43}$$

Fixed-time convergence: When $p_1 < 1$, we have $\gamma_2 > 1$, satisfying the dual-power condition. By Lemma 4, system achieves fixed-time convergence with settling time:

$$T_{\max} = \frac{1}{\alpha_1(1-\gamma_1)} + \frac{1}{\alpha_2(\gamma_2-1)}. \tag{44}$$

□

Remark 5. *The proof establishes rigorous convergence guarantees while acknowledging dimensional dependencies. The coefficients d^{-p_2} and potentially d^{p_1-2} may decrease with dimension, but remain positive. This can be compensated by appropriately choosing c_1, c_2.*

D EFToM: Detailed Convergence Proof

This appendix provides a detailed and self-contained proof of finite-/fixed-time convergence for the element-wise finite-/fixed-time optimizer with EMA momentum (EFToM) in continuous time.

Dynamics and notation. We study the EFToM system

$$\dot{\mathbf{w}} = -c_1 \operatorname{sign}(\mathbf{m}) \odot |\mathbf{m}|^{p_2} - c_2 \operatorname{sign}(\mathbf{m}) \odot |\mathbf{m}|^{2-p_1}, \tag{45a}$$

$$\dot{\mathbf{m}} = -\lambda\big(\mathbf{m} - \mathbf{g}\big), \qquad \mathbf{g} := \nabla\mathcal{L}(\mathbf{w}), \tag{45b}$$

with constants $c_1, c_2, \lambda > 0$ and exponents $p_2 \in (0,1)$, $p_1 \in (0,2)$. All pointwise operations ($|\cdot|^q$, $\operatorname{sign}(\cdot)$, $\odot$) are taken element-wise. To handle the non-smoothness at 0 (both for sign and the fractional powers), solutions are understood in the Carathéodory/Filippov sense; Lyapunov derivatives below are in the almost-everywhere (Filippov) sense.

Assumptions. We impose standard smoothness and Polyak-Łojasiewicz (PL) conditions, as stated in Assumption 1.

Shorthand and exponents. Let $:= \mathbf{m} - \mathbf{g}$ denote the momentum tracking error, and define

$$S_1 := \sum_{i=1}^{d} |m_i|^{1+p_2}, \qquad S_2 := \sum_{i=1}^{d} |m_i|^{3-p_1}, \quad \alpha := \tfrac{1+p_2}{2} \in \left(\tfrac{1}{2}, 1\right), \quad \beta := \tfrac{3-p_1}{2}. \tag{46}$$

D.1 Important Lemmas for EFToM

We consider the Lyapunov function

$$\mathcal{V}(\mathbf{w}, \mathbf{m}) := \mathcal{L}(\mathbf{w}) - \mathcal{L}^* + \kappa \|\mathbf{e}\|^2, \qquad \kappa > 0 \text{ to be chosen.} \tag{47}$$

Clearly $\mathcal{V} \geq 0$, and $\mathcal{V} = 0$ if $\mathcal{L}(\mathbf{w}) = \mathcal{L}^*$ and $\mathbf{e} = 0$. To prove the finite/fixed-time convergence, several lemmas are introduced:

Lemma 7. *Let $H := \nabla^2\mathcal{L}(\mathbf{w})$. Along equation 45,*

$$\dot{\mathcal{V}} = \mathbf{g}^\top \dot{\mathbf{w}} - 2\kappa\, \mathbf{e}^\top H\, \dot{\mathbf{w}} - 2\kappa\lambda \|\mathbf{e}\|^2. \tag{48}$$

Proof. By the chain rule, $\frac{d}{dt}(\mathcal{L}(\mathbf{w}) - \mathcal{L}^*) = \mathbf{g}^\top \dot{\mathbf{w}}$ and $\frac{d}{dt}\|\mathbf{e}\|^2 = 2\mathbf{e}^\top(\dot{\mathbf{m}} - \dot{\mathbf{g}}) = 2\mathbf{e}^\top(-\lambda\mathbf{e} - H\dot{\mathbf{w}})$. Combine the two identities and multiply the second by κ. □

For sake of simplicity, we introduce the element-wise maps $F(\mathbf{m}) := \operatorname{sign}(\mathbf{m}) \odot |\mathbf{m}|^{p_2}$ and $G(\mathbf{m}) := \operatorname{sign}(\mathbf{m}) \odot |\mathbf{m}|^{2-p_1}$. Since $\mathbf{g} = \mathbf{m} - \mathbf{e}$, it yeilds:

$$\begin{aligned} \mathbf{g}^\top \dot{\mathbf{w}} &= -c_1\, \mathbf{m}^\top F \;-\; c_2\, \mathbf{m}^\top G \;+\; c_1\, \mathbf{e}^\top F \;+\; c_2\, \mathbf{e}^\top G \\ &= -c_1 S_1 - c_2 S_2 + c_1\, \mathbf{e}^\top F + c_2\, \mathbf{e}^\top G. \end{aligned} \tag{49}$$

Now we will bound the $\mathbf{e}^\top F$, $\mathbf{e}^\top G$.

Lemma 8. *For any $\lambda > 0$, we have $c_1|\mathbf{e}^\top F| \;\le\; \frac{\kappa\lambda}{8}\,\|\mathbf{e}\|^2 + \frac{2c_1^2}{\kappa\lambda}\sum_{i=1}^d |m_i|^{2p_2}$, $\quad c_2|\mathbf{e}^\top G| \;\le\; \frac{\kappa\lambda}{8}\,\|\mathbf{e}\|^2 + \frac{2c_2^2}{\kappa\lambda}\sum_{i=1}^d |m_i|^{2(2-p_1)}$.*

Proof. Apply Cauchy–Schwarz and Young's inequality $|ab| \le \frac{\eta}{2}a^2 + \frac{1}{2\eta}b^2$ with $\eta = \kappa\lambda/4$ to $\mathbf{e}^\top F = \sum e_i\ \operatorname{sign}(m_i)|m_i|^{p_2}$ and to $\mathbf{e}^\top G = \sum e_i\ \operatorname{sign}(m_i)|m_i|^{\,2-p_1}$. □

Lemma 9. *Let $S_1 := \sum_{i=1}^d |m_i|^{\,1+p_2}$ and $S_2 := \sum_{i=1}^d |m_i|^{\,3-p_1}$ with $p_2 \in (0,1)$ and $p_1 < 2$. Define $\theta_1 := \frac{2p_2}{1+p_2} \in (0,1)$, $\quad \theta_2 := \frac{2(2-p_1)}{3-p_1}$. Then there exist constants $C_1, C_2 > 0$ depending only on (d, p_1, p_2) such that*

$$\sum_{i=1}^d |m_i|^{\,2p_2} \;\le\; d^{\,1-\theta_1}\, S_1^{\theta_1}, \tag{50}$$

and

$$\sum_{i=1}^d |m_i|^{\,2(2-p_1)} \;\le\; \begin{cases} d^{\,1-\theta_2}\, S_2^{\theta_2}, & \text{if } p_1 \ge 1 \ (\theta_2 \in (0,1]), \\ S_2^{\theta_2}, & \text{if } p_1 < 1 \ (\theta_2 > 1). \end{cases} \tag{51}$$

Proof. We use standard relations between ℓ^p quantities in $\mathbb{R}^d$:

(i) For $0 < r \le q$, $\|x\|_r \le d^{\,\frac{1}{r}-\frac{1}{q}}\,\|x\|_q$; hence $\sum |x_i|^{\,r} \le d^{\,1-\frac{r}{q}}\big(\sum |x_i|^{\,q}\big)^{\frac{r}{q}}$.

(ii) For $r \ge q > 0$, $\|x\|_r \le \|x\|_q$; hence $\sum |x_i|^{\,r} \le \big(\sum |x_i|^{\,q}\big)^{\frac{r}{q}}$.

Apply (i) to equation 50 with $q = 1 + p_2$, $r = 2p_2$ ($0 < r < q$), giving $\sum |m_i|^{2p_2} \le d^{\,1-\frac{2p_2}{1+p_2}}\big(\sum |m_i|^{1+p_2}\big)^{\frac{2p_2}{1+p_2}} = d^{\,1-\theta_1} S_1^{\theta_1}$. For equation 51, set $q = 3 - p_1$, $r = 2(2-p_1)$. If $p_1 \ge 1$ then $r \le q$, by using (i), we have $\sum |m_i|^r \le d^{\,1-\frac{r}{q}} S_2^{\frac{r}{q}} = d^{\,1-\theta_2} S_2^{\theta_2}$. If $p_1 < 1$, then $r > q$. By using (ii), we have $\sum |m_i|^r \le S_2^{\frac{r}{q}} = S_2^{\theta_2}$ □

Lemma 10. *For the EFToM system, we have*

$$-2\kappa\, \mathbf{e}^\top H \dot{\mathbf{w}} \;\le\; \frac{\kappa\lambda}{4}\|\mathbf{e}\|^2 + \frac{8\kappa L^2 c_1^2}{\lambda}\sum_{i=1}^d |m_i|^{2p_2} + \frac{8\kappa L^2 c_2^2}{\lambda}\sum_{i=1}^d |m_i|^{2(2-p_1)}. \tag{52}$$

Proof. Since $\|H\| \le L$, we have $|-2\kappa\, \mathbf{e}^\top H \dot{\mathbf{w}}| \;\le\; 2\kappa L \|\mathbf{e}\|\|\dot{\mathbf{w}}\| \;\le\; \frac{\kappa\lambda}{4}\|\mathbf{e}\|^2 + \frac{4\kappa L^2}{\lambda}\|\dot{\mathbf{w}}\|^2$. Now $\dot{\mathbf{w}} = -c_1 F(\mathbf{m}) - c_2 G(\mathbf{m})$, hence

$$\|\dot{\mathbf{w}}\|^2 \;\le\; 2c_1^2 \sum_{i=1}^d |m_i|^{2p_2} + 2c_2^2 \sum_{i=1}^d |m_i|^{2(2-p_1)}. \tag{53}$$

Substituting gives equation 52. □

Combining equation 48, equation 49, Lemma 8, and Lemma 10, we obtain

$$\dot{\mathcal{V}} \;\le\; -c_1 S_1 - c_2 S_2 - \tfrac{3}{2}\kappa\lambda\|\mathbf{e}\|^2 + \frac{K_1}{\lambda}\sum_{i=1}^d |m_i|^{2p_2} + \frac{K_2}{\lambda}\sum_{i=1}^d |m_i|^{2(2-p_1)}, \tag{54}$$

where $K_1 = \frac{2c_1^2}{\kappa} + 8\kappa L^2 c_1^2$, $K_2 = \frac{2c_2^2}{\kappa} + 8\kappa L^2 c_2^2$.

Proposition 1 (Net dissipation inequality)**.** *There exists a constant $\lambda_* > 0$ such that for all $\lambda \geq \lambda_*$, the Lyapunov derivative satisfies the following bounds.*

1. *If $p_1 \geq 1$ (so that $\theta_2 \in (0, 1]$), then*

$$\dot{\mathcal{V}} \;\leq\; -\tfrac{c_1}{2} S_1 \;-\; \tfrac{c_2}{2} S_2 \;-\; \tfrac{\kappa\lambda}{2} \|\mathbf{e}\|^2. \tag{55}$$

2. *If $p_1 < 1$ (so that $\theta_2 > 1$), then there exists $\hat{c}_2 > 0$ such that*

$$\dot{\mathcal{V}} \;\leq\; -\tfrac{c_1}{2} S_1 \;-\; \min\left\{ \tfrac{c_2}{2} S_2,\; \hat{c}_2\, S_2^{\theta_2} \right\} \;-\; \tfrac{\kappa\lambda}{2} \|\mathbf{e}\|^2, \tag{56}$$

with $\hat{c}_2 = \frac{c_2}{4}$.

Proof. Starting from Lemma 8 and Lemma 9, we obtain

$$\dot{\mathcal{V}} \;\leq\; -c_1 S_1 - c_2 S_2 - \kappa\lambda \|\mathbf{e}\|^2 + \frac{K_1}{\lambda} S_1^{\theta_1} + \frac{K_2}{\lambda} S_2^{\theta_2}, \tag{57}$$

where $K_1 = \frac{2c_1^2}{\kappa} + 8\kappa L^2 c_1^2$, $K_2 = \frac{2c_2^2}{\kappa} + 8\kappa L^2 c_2^2$, $\theta_1 = \frac{2p_2}{1+p_2} \in (0, 1)$, $\theta_2 = \frac{2(2-p_1)}{3-p_1}$.

Case (i): $p_1 \geq 1$. Here $\theta_2 \in (0, 1]$. By Young's inequality, for any $\varepsilon > 0$,

$$\frac{K_1}{\lambda} S_1^{\theta_1} \;\leq\; \varepsilon S_1 + C_1(\varepsilon)\lambda^{-\rho_1}, \qquad \frac{K_2}{\lambda} S_2^{\theta_2} \;\leq\; \varepsilon S_2 + C_2(\varepsilon)\lambda^{-\rho_2}, \tag{58}$$

for some exponents $\rho_1, \rho_2 > 0$. Choosing $\varepsilon = \frac{c_1}{2}, \frac{c_2}{2}$ respectively, and then taking

$$\lambda_* \;=\; \max\left\{ \left(\tfrac{4K_1}{c_1}\right)^{1-\theta_1},\; \left(\tfrac{4K_2}{c_2}\right)^{1-\theta_2} \right\}, \tag{59}$$

ensures that the small λ^{-1} remainders are absorbed, yielding equation 55.

Case (ii): $p_1 < 1$ (so $\theta_2 > 1$). In this case, the remainder involves a superlinear power $S_2^{\theta_2}$, $-c_2 S_2$ as $S_2 \to 0$. We thus argue in two regimes.

(a) Small S_2 regime. Choose $\lambda \geq \lambda_*$ such that $\frac{K_2}{\lambda} \leq c_2/2$. Then, for $S_2 \leq 1$,

$$-c_2 S_2 + \tfrac{K_2}{\lambda} S_2^{\theta_2} \;\leq\; -\tfrac{c_2}{2} S_2. \tag{60}$$

(b) Large S_2 regime. For $S_2 \geq 1$, since $\theta_2 > 1$, the term $S_2^{\theta_2}$ dominates the linear term, so that

$$-c_2 S_2 + \tfrac{K_2}{\lambda} S_2^{\theta_2} \;\leq\; -\hat{c}_2 S_2^{\theta_2}, \tag{61}$$

for some $\hat{c}_2 := \frac{c_2}{4} > 0$ (after enlarging λ_* to ensure $\frac{K_2}{\lambda} \leq \hat{c}_2$).

(c) Unified bound. Combining the two regimes, we obtain the global estimate

$$-c_2 S_2 + \tfrac{K_2}{\lambda} S_2^{\theta_2} \;\leq\; -\min\left\{ \tfrac{c_2}{2} S_2,\; \hat{c}_2 S_2^{\theta_2} \right\}. \tag{62}$$

Substituting this into the Lyapunov derivative together with the absorption of the S_1 remainder yields equation 56. □

Lemma 11. *Let $S_1 := \sum_{i=1}^d |m_i|^{1+p_2}$, $\quad S_2 := \sum_{i=1}^d |m_i|^{3-p_1}$, with $p_2 \in (0, 1)$ and $p_1 < 1$. Define the exponents $\alpha := \frac{1+p_2}{2} \in \left(\frac{1}{2}, 1\right)$, $\beta := 2 - p_1 > 1$, $\theta_2 := \frac{2(2-p_1)}{3-p_1} > 1$., Then there exist constants $\tilde{c}_{1d}, \tilde{c}_{2d} > 0$ (depending on d, p_1, p_2, μ, κ) such that*

$$S_1 \;\geq\; \tilde{c}_{1d}\, \mathcal{V}^{\alpha} \;-\; \tfrac{\kappa\lambda}{4} \|\mathbf{e}\|^2, \tag{63}$$

$$S_2^{\theta_2} \;\geq\; \tilde{c}_{2d}\, \mathcal{V}^{\beta} \;-\; \tfrac{\kappa\lambda}{4} \|\mathbf{e}\|^2. \tag{64}$$

Proof. Recall $\mathbf{m} = \mathbf{g} + \mathbf{e}$, where $\mathbf{g} = \nabla\mathcal{L}(\mathbf{w})$ and $\mathbf{e} = \mathbf{m} - \mathbf{g}$.

First, we bound S_1. By ℓ^p–norm monotonicity and Jensen's inequality, $S_1 \geq \|\mathbf{m}\|^{1+p_2} = \|\mathbf{g}+\mathbf{e}\|^{1+p_2}$. If $\|\mathbf{e}\| \leq \frac{1}{2}\|\mathbf{g}\|$, then $\|\mathbf{m}\| \geq \|\mathbf{g}\| - \|\mathbf{e}\| \geq \frac{1}{2}\|\mathbf{g}\|$, so

$$S_1 \;\geq\; 2^{-(1+p_2)}\|\mathbf{g}\|^{1+p_2}. \tag{65}$$

From the PL inequality, it gives $\|\mathbf{g}\|^2 \geq 2\mu\big(\mathcal{V} - \kappa\|\mathbf{e}\|^2\big)$. To complete this proof, two cases are considered:

1. If $\|\mathbf{e}\| \leq \frac{1}{2}\|\mathbf{g}\|$, the negative term $-\kappa\|\mathbf{e}\|^2$ can be absorbed into $\frac{1}{2}\|\mathbf{g}\|^2$, yielding $\|\mathbf{g}\|^2 \geq \frac{2\mu}{1+\frac{\mu\kappa}{2}}\,\mathcal{V}$. Therefore,

$$S_1 \;\geq\; 2^{-(1+p_2)}\Big(\frac{2\mu}{1+\frac{\mu\kappa}{2}}\Big)^{\alpha}\mathcal{V}^{\alpha}. \tag{66}$$

2. If $\|\mathbf{e}\| \geq \frac{1}{2}\|\mathbf{g}\|$, then $\mathcal{V} \geq \kappa\|\mathbf{e}\|^2$ dominates, and the error term can be absorbed into the existing $-\frac{\kappa\lambda}{4}\|\mathbf{e}\|^2$ contribution in $\dot{\mathcal{V}}$. Thus, in both regimes,

$$S_1 \;\geq\; \tilde{c}_{1d}\,\mathcal{V}^{\alpha} - \tfrac{\kappa\lambda}{4}\|\mathbf{e}\|^2, \qquad \tilde{c}_{1d} := 2^{-(1+p_2)}\Big(\frac{2\mu}{1+\frac{\mu\kappa}{2}}\Big)^{\alpha}. \tag{67}$$

Next, we will bound S_2. By definition, $S_2^{\theta_2} = \|\mathbf{m}\|^{2(2-p_1)} = \|\mathbf{g}+\mathbf{e}\|^{2\beta}$. If $\|\mathbf{e}\| \leq \frac{1}{2}\|\mathbf{g}\|$. Then $S_2^{\theta_2} \geq 2^{-2\beta}\,\|\mathbf{g}\|^{2\beta}$. From PL condition we have $\|\mathbf{g}\|^2 \geq 2\mu\big(\mathcal{V} - \kappa\|\mathbf{e}\|^2\big)$. As before, the $-\kappa\|\mathbf{e}\|^2$ term can be absorbed into $\frac{1}{2}\|\mathbf{g}\|^2$, yielding $\|\mathbf{g}\|^2 \geq \frac{2\mu}{1+\frac{\mu\kappa}{2}}\,\mathcal{V}$. Therefore,

$$S_2^{\theta_2} \;\geq\; 2^{-2\beta}\Big(\frac{2\mu}{1+\frac{\mu\kappa}{2}}\Big)^{\beta}\mathcal{V}^{\beta}. \tag{68}$$

If $\|\mathbf{e}\| \geq \frac{1}{2}\|\mathbf{g}\|$. Here $\mathcal{V} \geq \kappa\|\mathbf{e}\|^2$, so that $\|\mathbf{e}\|^{2\beta} \leq \kappa^{-\beta}\mathcal{V}^{\beta}$. Thus any positive error terms of type $\|\mathbf{e}\|^{2\beta}$ can be absorbed into either $\mathcal{V}^{\beta}$ or into the negative contribution $-\frac{\kappa\lambda}{4}\|\mathbf{e}\|^2$ in $\dot{\mathcal{V}}$. Combining both regimes, we obtain

$$S_2^{\theta_2} \;\geq\; \tilde{c}_{2d}\,\mathcal{V}^{\beta} - \tfrac{\kappa\lambda}{4}\|\mathbf{e}\|^2, \qquad \tilde{c}_{2d} := 2^{-2\beta}\Big(\frac{2\mu}{1+\frac{\mu\kappa}{2}}\Big)^{\beta}. \tag{69}$$

This proves equation 63–equation 64. □

D.2 Finite-/Fixed-Time Convergence of EFToM

Based on the above analysis, we give the formal convergence of the EFToM dynamic system (45).

Theorem 4 (Finite-/Fixed-time convergence of EFToM)**.** *Suppose Assumption 1 holds and choose $\lambda \geq \lambda_*$ from Proposition 1. Then every trajectory of equation 45 converges to the global optimum in finite or fixed time, depending on p_1.*

1. ***Case A** ($p_1 \geq 1$)**: Finite-time convergence.** From Proposition 1 (case (i)) and Lemma 11, there exist constants*

$$a := \tfrac{c_1}{2}\,2^{-(1+p_2)}\Big(\tfrac{2\mu}{1+\frac{\mu\kappa}{2}}\Big)^{\alpha}, \qquad b := \tfrac{c_2}{2}\,2^{-(3-p_1)}\Big(\tfrac{2\mu}{1+\frac{\mu\kappa}{2}}\Big)^{\beta},$$

where $\alpha = \frac{1+p_2}{2} \in (\frac{1}{2}, 1)$, $\beta = \frac{3-p_1}{2} \in (0, 1]$. Then for almost all t,

$$\dot{\mathcal{V}}(t) \;\leq\; -a\,\mathcal{V}(t)^{\alpha} \;-\; b\,\mathcal{V}(t)^{\beta}. \tag{70}$$

Consequently, the settling time is finite and satisfies

$$T(\mathcal{V}(0)) \;\leq\; \frac{\mathcal{V}(0)^{\,1-\alpha}}{a(1-\alpha)} \;+\; 1_{\{\beta<1\}}\,\frac{\mathcal{V}(0)^{\,1-\beta}}{b(1-\beta)}. \tag{71}$$

2. ***Case B*** *($p_1 < 1$)**: Fixed-time convergence.** If $p_1 < 1$, then $\alpha = \frac{1+p_2}{2} \in (\frac{1}{2}, 1)$, $\beta = 2 - p_1 > 1$. Then for almost all t,*

$$\dot{\mathcal{V}}(t) \;\le\; -a\,\mathcal{V}(t)^{\alpha} \;-\; b\,\mathcal{V}(t)^{\beta}. \tag{72}$$

Consequently, the settling time is bounded uniformly (independent of $\mathcal{V}(0)$) by

$$T_{\max} \;\le\; \frac{1}{a(1-\alpha)} + \frac{1}{b(\beta-1)}. \tag{73}$$

In both cases, convergence of $\mathcal{V}$ yields global optimality.

Proof of Theorem 4. We start from Proposition 1, which already gives for $\lambda \ge \lambda_*$:

$$\text{(Case A, } p_1 \ge 1\text{):} \quad \dot{\mathcal{V}} \;\le\; -\tfrac{c_1}{2} S_1 - \tfrac{c_2}{2} S_2 - \tfrac{\kappa\lambda}{2}\|\mathbf{e}\|^2, \tag{74}$$

$$\text{(Case B, } p_1 < 1\text{):} \quad \dot{\mathcal{V}} \;\le\; -\tfrac{c_1}{2} S_1 - \min\Big\{\tfrac{c_2}{2} S_2,\; \hat{c}_2 S_2^{\theta_2}\Big\} - \tfrac{\kappa\lambda}{2}\|\mathbf{e}\|^2, \tag{75}$$

where $\hat{c}_2 = \frac{c_2}{4}$ and $\theta_2 = \frac{2(2-p_1)}{3-p_1}$.

For $p_1 < 1$, Lemma 11 yields

$$S_1 \;\ge\; \tilde{c}_{1d}\,\mathcal{V}^{\alpha} - \tfrac{\kappa\lambda}{4}\|\mathbf{e}\|^2, \tag{76}$$

$$S_2^{\theta_2} \;\ge\; \tilde{c}_{2d}\,\mathcal{V}^{\beta} - \tfrac{\kappa\lambda}{4}\|\mathbf{e}\|^2, \tag{77}$$

with $\tilde{c}_{1d} = 2^{-(1+p_2)}\Big(\frac{2\mu}{1+\frac{\mu\kappa}{2}}\Big)^{\alpha}$, $\tilde{c}_{2d} = 2^{-2\beta}\Big(\frac{2\mu}{1+\frac{\mu\kappa}{2}}\Big)^{\beta}$, and exponents $\alpha = \frac{1+p_2}{2} \in (\frac{1}{2}, 1)$, $\beta = 2 - p_1 > 1$.

For $p_1 \ge 1$, a parallel argument (using the ℓ^p monotonicity as in Lemma 11) gives

$$S_1 \;\ge\; \tilde{c}_{1d}\,\mathcal{V}^{\alpha} - \tfrac{\kappa\lambda}{4}\|\mathbf{e}\|^2, \qquad S_2 \;\ge\; \tilde{c}_{2d}\,\mathcal{V}^{\beta} - \tfrac{\kappa\lambda}{4}\|\mathbf{e}\|^2, \tag{78}$$

with the same $\tilde{c}_{1d}$ but now $\tilde{c}_{2d} = 2^{-(3-p_1)}\Big(\frac{2\mu}{1+\frac{\mu\kappa}{2}}\Big)^{\beta}$, $\beta = \frac{3-p_1}{2} \in (0, 1]$.

Case A ($p_1 \ge 1$). Substituting the lower bounds into equation 74 and absorbing the $-\frac{\kappa\lambda}{4}\|\mathbf{e}\|^2$ contributions, we obtain

$$\dot{\mathcal{V}} \;\le\; -\tfrac{c_1}{2}\,\tilde{c}_{1d}\,\mathcal{V}^{\alpha} - \tfrac{c_2}{2}\,\tilde{c}_{2d}\,\mathcal{V}^{\beta}. \tag{79}$$

Thus equation 70 holds with $a = \frac{c_1}{2}\,\tilde{c}_{1d}$, $b = \frac{c_2}{2}\,\tilde{c}_{2d}$.

Case B ($p_1 < 1$). In the large-S_2 regime, equation 75 gives the $-\hat{c}_2 S_2^{\theta_2}$ dissipation. Using Lemma 11, we convert this into

$$-\hat{c}_2 S_2^{\theta_2} \;\le\; -\hat{c}_2\tilde{c}_{2d}\,\mathcal{V}^{\beta} + \tfrac{\kappa\lambda}{4}\|\mathbf{e}\|^2. \tag{80}$$

Absorbing the error term and combining with the S_1 estimate, we obtain

$$\dot{\mathcal{V}} \;\le\; -\tfrac{c_1}{2}\,\tilde{c}_{1d}\,\mathcal{V}^{\alpha} - \hat{c}_2\tilde{c}_{2d}\,\mathcal{V}^{\beta}, \tag{81}$$

so that equation 72 holds with $a = \frac{c_1}{2}\,\tilde{c}_{1d}$, $b = \hat{c}_2\,\tilde{c}_{2d}$.

Now $\dot{\mathcal{V}} \le -a\mathcal{V}^{\alpha} - b\mathcal{V}^{\beta}$ with explicit $a, b > 0$. If $0 < \beta \le 1$ (Case A), Lemma 3 yields finite-time convergence with settling time bounded as in equation 71. If $\beta > 1$ (Case B), Lemma 4 ensures fixed-time convergence with a uniform bound equation 73. Finally, under the PL condition, $\mathcal{V} = 0$ implies $\mathcal{L}(\mathbf{w}) = \mathcal{L}^*$ and $\mathbf{e} = 0$, hence global optimality is achieved. □

E Proof of Convergence for PEFToM

We provide a complete proof of finite-/fixed-time convergence for the Polyak momentum EFToM (PEFToM) dynamics. Note that the proof process is quite like that of EFToM.

E.1 PEFToM Dynamics

The PEFToM dynamics are

$$\dot{\mathbf{v}} = \mathbf{g} - \gamma \mathbf{v}, \qquad \mathbf{g} := \nabla \mathcal{L}(\mathbf{w}), \tag{82a}$$

$$\dot{\mathbf{w}} = -c_1 \, \mathrm{sign}(\mathbf{v}) \odot |\mathbf{v}|^{p_2} - c_2 \, \mathrm{sign}(\mathbf{v}) \odot |\mathbf{v}|^{2-p_1}, \tag{82b}$$

with parameters $c_1, c_2, \gamma > 0$, $p_2 \in (0,1)$, $p_1 \in (0,2)$.

Define the scaled tracking error

$$\mathbf{e} := \mathbf{v} - \tfrac{1}{\gamma}\mathbf{g}. \tag{83}$$

Then

$$\dot{\mathbf{e}} = -\gamma \mathbf{e} - \tfrac{1}{\gamma} H \dot{\mathbf{w}}, \qquad H := \nabla^2 \mathcal{L}(\mathbf{w}). \tag{84}$$

E.2 Lyapunov function

We introduce the Lyapunov function: $\mathcal{V}(\mathbf{w}, \mathbf{v}) := \mathcal{L}(\mathbf{w}) - \mathcal{L}^* + \kappa \|\mathbf{e}\|^2$, for some $\kappa > 0$. Therefore:

$$\begin{aligned} \dot{\mathcal{V}} &= \mathbf{g}^\top \dot{\mathbf{w}} + 2\kappa \mathbf{e}^\top \dot{\mathbf{e}} \\ &= \mathbf{g}^\top \dot{\mathbf{w}} + 2\kappa \mathbf{e}^\top \big(-\gamma \mathbf{e} - \tfrac{1}{\gamma} H \dot{\mathbf{w}} \big). \\ &= \mathbf{g}^\top \dot{\mathbf{w}} - 2\kappa\gamma \|\mathbf{e}\|^2 - \tfrac{2\kappa}{\gamma} \mathbf{e}^\top H \end{aligned} \tag{85}$$

Now we will bound $g^\top \dot{\mathbf{w}}$. Let $F(\mathbf{v}) := \mathrm{sign}(\mathbf{v}) \odot |\mathbf{v}|^{p_2}$, $\quad G(\mathbf{v}) := \mathrm{sign}(\mathbf{v}) \odot |\mathbf{v}|^{2-p_1}$. Then $\dot{\mathbf{w}} = -c_1 F - c_2 G$. Moreover $\mathbf{g} = \gamma \mathbf{v} - \gamma \mathbf{e}$, hence

$$\begin{aligned} \mathbf{g}^\top \dot{\mathbf{w}} &= (\gamma \mathbf{v} - \gamma \mathbf{e})^\top \dot{\mathbf{w}} \\ &= -\gamma c_1 \mathbf{v}^\top F - \gamma c_2 \mathbf{v}^\top G + \gamma c_1 \mathbf{e}^\top F + \gamma c_2 \mathbf{e}^\top G. \end{aligned} \tag{86}$$

Since $\mathbf{v}^\top F = \sum_i |v_i|^{1+p_2}$ and $\mathbf{v}^\top G = \sum_i |v_i|^{3-p_1}$, we define $S_1 := \sum_{i=1}^d |v_i|^{1+p_2}$, $S_2 := \sum_{i=1}^d |v_i|^{3-p_1}$, so that

$$\mathbf{g}^\top \dot{\mathbf{w}} = -\gamma c_1 S_1 - \gamma c_2 S_2 + \gamma c_1 \mathbf{e}^\top F + \gamma c_2 \mathbf{e}^\top G. \tag{87}$$

Terms $\mathbf{e}^\top F$ and $\mathbf{e}^\top G$ can be bounded by Cauchy–Schwarz and Young,

$$\gamma c_1 |\mathbf{e}^\top F| \le \gamma c_1 \|\mathbf{e}\| \|F\| \le \tfrac{\kappa\gamma}{8} \|\mathbf{e}\|^2 + \tfrac{2c_1^2}{\kappa} \|F\|^2, \tag{88}$$

$$\gamma c_2 |\mathbf{e}^\top G| \le \tfrac{\kappa\gamma}{8} \|\mathbf{e}\|^2 + \tfrac{2c_2^2}{\kappa} \|G\|^2. \tag{89}$$

Note that $\|F\|^2 = \sum |v_i|^{2p_2}$, $\|G\|^2 = \sum |v_i|^{2(2-p_1)}$.

Now we will bound $-\frac{2\kappa}{\gamma} \mathbf{e}^\top H \dot{\mathbf{w}}$. Since $||H|| \le L$, we have

$$-\tfrac{2\kappa}{\gamma} \mathbf{e}^\top H \dot{\mathbf{w}} \le \tfrac{2\kappa L}{\gamma} \|\mathbf{e}\| \|\dot{\mathbf{w}}\| \le \tfrac{\kappa\gamma}{4} \|\mathbf{e}\|^2 + \tfrac{4\kappa L^2}{\gamma^2} \|\dot{\mathbf{w}}\|^2. \tag{90}$$

Since $\dot{\mathbf{w}} = -c_1 F - c_2 G$, we have $\|\dot{\mathbf{w}}\|^2 \le 2c_1^2 \|F\|^2 + 2c_2^2 \|G\|^2$. Substitute it to (90), it yields,

$$-\tfrac{2\kappa}{\gamma} \mathbf{e}^\top H \dot{\mathbf{w}} \le \tfrac{\kappa\gamma}{4} \|\mathbf{e}\|^2 + \tfrac{4\kappa L^2}{\gamma^2} (2c_1^2 \|F\|^2 + 2c_2^2 \|G\|^2) \tag{91}$$

Substitute (91), (88), (89), and (87) to (85), it yeilds:

$$\dot{\mathcal{V}} \le -\gamma c_1 S_1 - \gamma c_2 S_2 - \tfrac{3}{2} \kappa\gamma \|\mathbf{e}\|^2 + \tilde{c}_1 \|F\|^2 + \tilde{c}_2 \|G\|^2, \tag{92}$$

where $\tilde{c}_1 = \frac{2c_1^2}{\kappa} + \frac{8\kappa L^2}{\gamma^2} c_1^2, \quad \tilde{c}_2 = \frac{2c_2^2}{\kappa} + \frac{8\kappa L^2}{\gamma^2} c_2^2$.

E.3 INTERPOLATION INEQUALITIES

Following the interpolation bounds in Lemma 9, we have

$$\|F(\mathbf{v})\|^2 = \sum_{i=1}^{d} |v_i|^{2p_2} \le d^{1-\theta_1} S_1^{\theta_1}, \quad \theta_1 = \frac{2p_2}{1+p_2} \in (0,1), \tag{93}$$

$$\|G(\mathbf{v})\|^2 = \sum_{i=1}^{d} |v_i|^{2(2-p_1)} \le \begin{cases} d^{1-\theta_2} S_2^{\theta_2}, & p_1 \ge 1, \\ S_2^{\theta_2}, & p_1 < 1, \end{cases} \quad \theta_2 = \frac{2(2-p_1)}{3-p_1}. \tag{94}$$

Substituting (93)–(94) into the bound

$$\dot{\mathcal{V}} \le -\gamma c_1 S_1 - \gamma c_2 S_2 - \tfrac{3}{2}\kappa\gamma\|\mathbf{e}\|^2 + \tilde{c}_1\|F\|^2 + \tilde{c}_2\|G\|^2, \tag{95}$$

we obtain

$$\dot{\mathcal{V}} \le -\gamma c_1 S_1 - \gamma c_2 S_2 - \tfrac{3}{2}\kappa\gamma\|\mathbf{e}\|^2 + \tilde{c}_1 d^{1-\theta_1} S_1^{\theta_1} + \tilde{c}_2 \cdot \begin{cases} d^{1-\theta_2} S_2^{\theta_2}, & p_1 \ge 1, \\ S_2^{\theta_2}, & p_1 < 1. \end{cases} \tag{96}$$

Proposition 2 (Net dissipation inequality for PEFToM)**.** *There exists a constant $\gamma_\star > 0$ such that for all $\gamma \ge \gamma_\star$, the Lyapunov derivative along equation 82 satisfies:*

1. *If $p_1 \ge 1$ (so that $\theta_2 \in (0,1]$), then*
$$\dot{\mathcal{V}} \;\le\; -\tfrac{\gamma c_1}{2} S_1 - \tfrac{\gamma c_2}{2} S_2 - \tfrac{\kappa\gamma}{2}\|\mathbf{e}\|^2. \tag{97}$$
2. *If $p_1 < 1$ (so that $\theta_2 > 1$), then there exists $\hat{c}_2 > 0$ such that*
$$\dot{\mathcal{V}} \;\le\; -\tfrac{\gamma c_1}{2} S_1 - \min\left\{ \tfrac{\gamma c_2}{2} S_2,\; \hat{c}_2 S_2^{\theta_2} \right\} - \tfrac{\kappa\gamma}{2}\|\mathbf{e}\|^2, \tag{98}$$
with $\hat{c}_2 = \frac{\gamma c_2}{4}$.

Proof. Starting from equation 96, we have

$$\dot{\mathcal{V}} \le -\gamma c_1 S_1 - \gamma c_2 S_2 - \tfrac{3}{2}\kappa\gamma\|\mathbf{e}\|^2 + \tilde{c}_1 d^{1-\theta_1} S_1^{\theta_1} + \tilde{c}_2 \cdot \begin{cases} d^{1-\theta_2} S_2^{\theta_2}, & p_1 \ge 1, \\ S_2^{\theta_2}, & p_1 < 1. \end{cases}$$

Case (i): $p_1 \ge 1$ ($\theta_2 \in (0,1]$). By Young's inequality, for any $\varepsilon > 0$,

$$\tilde{c}_1 d^{1-\theta_1} S_1^{\theta_1} \;\le\; \varepsilon S_1 + C_1(\varepsilon)\gamma^{-\rho_1}, \qquad \tilde{c}_2 d^{1-\theta_2} S_2^{\theta_2} \;\le\; \varepsilon S_2 + C_2(\varepsilon)\gamma^{-\rho_2}, \tag{99}$$

for some exponents $\rho_1, \rho_2 > 0$. Choosing $\varepsilon = \frac{\gamma c_1}{2}$ and $\varepsilon = \frac{\gamma c_2}{2}$, and taking γ sufficiently large to absorb the remainders, we obtain

$$\dot{\mathcal{V}} \;\le\; -\tfrac{\gamma c_1}{2} S_1 - \tfrac{\gamma c_2}{2} S_2 - \tfrac{\kappa\gamma}{2}\|\mathbf{e}\|^2, \tag{100}$$

which is equation 97.

Case (ii): $p_1 < 1$ ($\theta_2 > 1$). In this case, the remainder term is superlinear in S_2. We split the analysis into two regimes:

(a) Small S_2. Choose γ large enough so that $\tilde{c}_2 \le \frac{\gamma c_2}{2}$. Then, for $S_2 \le 1$,

$$-\gamma c_2 S_2 + \tilde{c}_2 S_2^{\theta_2} \;\le\; -\tfrac{\gamma c_2}{2} S_2. \tag{101}$$

(b) Large S_2. For $S_2 \ge 1$, since $\theta_2 > 1$, the term $S_2^{\theta_2}$ dominates S_2, and hence

$$-\gamma c_2 S_2 + \tilde{c}_2 S_2^{\theta_2} \;\le\; -\hat{c}_2 S_2^{\theta_2}, \tag{102}$$

for some $\hat{c}_2 := \frac{\gamma c_2}{4} > 0$, after possibly enlarging γ so that $\tilde{c}_2 \le \hat{c}_2$.

(c) Unified bound. Combining the two regimes, we obtain

$$-\gamma c_2 S_2 + \tilde{c}_2 S_2^{\theta_2} \;\le\; -\min\left\{ \tfrac{\gamma c_2}{2} S_2,\; \hat{c}_2 S_2^{\theta_2} \right\}. \tag{103}$$

Substituting into the Lyapunov derivative yields

$$\dot{\mathcal{V}} \;\le\; -\tfrac{\gamma c_1}{2} S_1 - \min\left\{ \tfrac{\gamma c_2}{2} S_2,\; \hat{c}_2 S_2^{\theta_2} \right\} - \tfrac{\kappa\gamma}{2}\|\mathbf{e}\|^2, \tag{104}$$

which is equation 98. □

E.4 FINITE-/FIXED-TIME CONVERGENCE OF PEFTOM

The proof strategy is entirely analogous to that of EFToM (Theorem 4). In particular, starting from the dissipation inequality (Proposition 2), and combining with the interpolation bounds (Lemma 9) and Lemma 11, we obtain a Lyapunov decay of the form

$$\dot{\mathcal{V}} \;\le\; -a\mathcal{V}^{\alpha} - b\mathcal{V}^{\beta},$$

with the same exponents (α, β) and constants $(\hat{a}, \hat{b})$ up to replacing λ by γ. Therefore, the finite-/fixed-time convergence result for EFToM extends directly to PEFToM, with explicit constants summarized below.

Theorem 5 (PEFToM Finite-/Fixed-Time Convergence)**.** *Consider the PEFToM dynamics equation 82 with parameters $p_2 \in (0,1)$, $0 < p_1 < 2$, and $c_1, c_2, \gamma > 0$. Under Assumption 1, choose $\gamma \ge \gamma_\star$ with*

$$\gamma_\star := \max\left\{ \left(4\gamma_0 \tilde{K}_g\right)^{\frac{1}{2-\theta}},\ \frac{4C_\kappa}{\gamma_0} \right\}, \qquad \gamma_0 := \tfrac{c_1}{2}, \quad \theta := 2 - q_{\max}, \quad q_{\max} := \max\{p_2,\, 2-p_1\}, \tag{105}$$

where $\tilde{K}_g, C_\kappa > 0$ are explicit constants given in the proof.

Define the exponents

$$\alpha := \tfrac{1+p_2}{2} \in \left(\tfrac{1}{2}, 1\right), \qquad \beta := \begin{cases} \frac{3-p_1}{2}, & 1 \le p_1 < 2, \\ 2 - p_1, & 0 < p_1 < 1. \end{cases}$$

Then the following convergence guarantees hold:

(i) ***Finite-time convergence*** *($1 \le p_1 < 2$, equivalently $\beta \le 1$): For any initial state $(\mathbf{w}(0), \mathbf{v}(0))$, the trajectory converges within time*

$$T \;\le\; \frac{V_{\mathrm{tot}}(0)^{\,1-\alpha}}{\hat{a}(1-\alpha)} + \frac{V_{\mathrm{tot}}(0)^{\,1-\beta}}{\hat{b}(1-\beta)}, \tag{106}$$

where $V_{\mathrm{tot}}(0) := \mathcal{L}(\mathbf{w}(0)) - \mathcal{L}^* + \gamma_0 \left\| \mathbf{v}(0) - \frac{1}{\gamma}\mathbf{g}(0) \right\|^2$.

(ii) ***Fixed-time convergence*** *($0 < p_1 < 1$, equivalently $\beta > 1$): Every trajectory reaches the global optimum $(\mathbf{w}^\star, \mathbf{0})$ within a uniform bound*

$$T_{\max} \;=\; \frac{1}{\hat{a}(1-\alpha)} + \frac{1}{\hat{b}(\beta-1)}, \tag{107}$$

where $\hat{a} := \frac{1}{2}c_1\gamma d^{-\frac{1-p_2}{2}}(2\mu)^{\alpha}$, $\hat{b} := \frac{1}{2}\gamma c_2 d^{-\frac{1-p_1}{2}}(2\mu)^{\beta}$.

Remark 6 (Role of γ versus λ)**.** *In EFToM, the negative dissipation terms are proportional to $\lambda_0 c_1 S_1$ and $\lambda_0 c_2 S_2$, so that the effective constants $\hat{a}, \hat{b}$ do not explicitly depend on λ, and λ only appears through the admissibility condition $\lambda \ge \lambda_\star$. In contrast, for PEFToM the dissipation terms scale as $\gamma c_1 S_1$ and $\gamma c_2 S_2$, so the convergence coefficients $\hat{a}, \hat{b}$ inherit a linear dependence on γ: $\hat{a} = \frac{\gamma}{2}c_1 d^{-\frac{1-p_2}{2}}(2\mu)^{\alpha}$, $\hat{b} = \frac{\gamma}{2}c_2 d^{-\frac{1-p_1}{2}}(2\mu)^{\beta}$. Thus, in PEFToM, the choice of a larger γ not only guarantees admissibility ($\gamma \ge \gamma_\star$) but also strengthens the dissipation rate in the Lyapunov inequality, leading to smaller convergence time bounds.*

F HYPERPARAMETER

We follow the setting in Zhuang et al. (2020). For AdamW and AdaBelief, the default parameter are used: $\beta_1 = 0.9$, $\beta_2 = 0.999$, $\epsilon = 10^{-8}$, learning rate is 0.001, and the weight decay is set to 5×10^{-4}. For SignSGD, Signum and Lion, we search the learning rate among $\eta \in \{0.00001, 0.00005, 0.0001, 0.0005, 0.001, 0.005, 0.01, 0.05\}$, and set $\beta = 0.9$ for Signum. For SGD, SGDM we search the learning rate among $\eta \in \{0.001, 0.005, 0.01, 0.05, 0.1\}$. The model is trained for 200 epochs with a batch size of 128, and the learning rate is multiplied by 0.1 at epoch 150. The details hyperparameters used in the experiment are given in Table 3, 4, 5.

Remark 7. *Our experimental evaluations primarily explore the finite-time convergence regime ($p_1 \geq 1$) rather than the fixed-time regime ($p_1 < 1$). While fixed-time convergence provides stronger theoretical guarantees, we observed that $p_1 < 1$ parameters exhibit higher sensitivity to discretization effects and step size choices, potentially leading to training instability. This discretization gap between continuous-time theory and discrete implementation represents a common challenge in translating control-theoretic results to practical optimization algorithms. The finite-time variants ($p_1 \geq 1$) demonstrate more robust behavior under standard stochastic training conditions while still providing significant convergence acceleration.*

Table 3: CIFAR10 Hyperparameters

Model	optimizer	batch size	learning rate	schedule	p_1	p_2	β_1	β_2	λ
VGG11/Resnet34/Densenet121	SGD	128	0.01	step	-	-	-	-	5e-4
VGG11/Resnet34/Densenet121	SGDM	128	0.01	step	-	-	0.9	-	5e-4
VGG11/Resnet34/Densenet121	SignSGD	128	1e-4	step	-	-	-	-	5e-4
VGG11/Resnet34/Densenet121	Signum	128	1e-4	step	-	-	0.9	-	5e-4
Resnet34/Densenet121	Lion	128	5e-5	step	-	-	0.95	0.98	5e-4
Resnet34/Densenet121	EFT	128	0.01	step	-	0.6	-	-	5e-4
Resnet34/Densenet121	EFToM	128	0.01	step	-	0.6	0.9	-	5e-4
VGG11/Resnet34/Densenet121	PEFToM	128	0.01	step	-	0.9	0.9	-	5e-4
VGG11/Resnet34/Densenet121	FxTS-GF(M)	128	0.01	step	20	1.98	0.9	-	5e-4
VGG11/Resnet34/Densenet121	AdamW	128	0.001	step	-	-	0.9	0.999	5e-4
VGG11/Resnet34/Densenet121	AdaBelief	128	0.001	step	-	-	0.9	0.999	5e-4
VGG11	Lion	128	1e-5	step	-	-	0.95	0.98	5e-4
VGG11	EFT	128	0.01	step	-	0.8	-	-	5e-4
VGG11	EFToM	128	0.01	step	-	0.8	0.9	-	5e-4

Table 4: CIFAR100 Hyperparameters

Model	optimizer	batch size	learning rate	schedule	p_1	p_2	β_1	β_2	λ
VGG11/Resnet34/Densenet121	SGD	128	0.1	step	-	-	-	-	5e-4
VGG11/Resnet34/Densenet121	SGDM	128	0.01	step	-	-	0.9	-	5e-4
VGG11/Resnet34	SignSGD	128	5e-5	step	-	-	-	-	5e-4
VGG11/Resnet34	Signum	128	5e-5	step	-	-	0.9	-	5e-4
Resnet34/Densenet121	Lion	128	5e-5	step	-	-	0.95	0.98	5e-4
VGG11/Resnet34	EFT	128	0.1	step	-	0.9	-	-	5e-4
VGG11/Resnet34	EFToM	128	0.1	step	-	0.9	0.9	-	5e-4
VGG11/Resnet34/Densenet121	PEFToM	128	0.01	step	-	0.8	0.9	-	5e-4
VGG11/Resnet34/Densenet121	FxTS-GF(M)	128	0.05	step	20	1.98	0.9	-	5e-4
VGG11/Resnet34/Densenet121	AdamW	128	0.001	step	-	-	0.9	0.999	5e-4
VGG11/Resnet34/Densenet121	AdaBelief	128	0.001	step	-	-	0.9	0.999	5e-4
Densenet121	SignSGD	128	1e-4	step	-	-	-	-	5e-4
Densenet121	Signum	128	1e-4	step	-	-	-	-	5e-4
VGG11	Lion	128	1e-5	step	-	-	0.95	0.98	5e-4
Densenet121	EFT	128	0.1	step	-	0.8	-	-	5e-4
Densenet121	EFToM	128	0.1	step	-	0.8	0.9	-	5e-4

Table 5: C4 Hyperparameters

Model	optimizer	batch size	learning rate	schedule	p_1	p_2	β_1	β_2	λ
Llama 60M	SGD	16	0.2	cosine	-	-	-	-	5e-4
Llama 60M	SGDM	16	0.1	cosine	-	-	0.9	-	5e-4
Llama 60M	SignSGD	16	0.001	cosine	-	-	-	-	5e-4
Llama 60M	Signum	16	0.0001	cosine	-	-	0.9	-	5e-4
Llama 60M	EFT	16	0.002	cosine	0.98	0.2	-	-	5e-4
Llama 60M	EFToM	16	0.002	cosine	0.98	0.2	0.9	-	5e-4
Llama 60M	PEFToM	16	0.1	cosine	-	0.8	0.9	-	5e-4
Llama 60M	FxTS-GF(M)	16	0.1	cosine	20	1.98	0.9	-	5e-4
Llama 60M	AdamW	16	0.001	cosine	-	-	0.9	0.999	5e-4
Llama 60M	AdaBelief	16	0.001	cosine	-	-	0.9	0.999	5e-4
Llama 60M	Lion	16	0.0001	cosine	-	-	0.95	0.98	5e-4

G INFLUENCE OF PARAMETER p_2

To investigate the impact of the finite-time parameter p_2 on optimization performance, we conduct comprehensive ablation studies across diverse tasks: CIFAR-10/100 using PEFToM with $p_2 \in \{0.4, 0.5, 0.6, 0.7, 0.8, 0.9\}$, and C4 language modeling using EFToM with $p_2 \in \{0.1, 0.2, 0.3, 0.4, 0.5, 0.6\}$.

The results reveal striking task-dependent parameter sensitivity patterns that illuminate the relationship between theoretical predictions and practical performance. On vision tasks (Figures 5 and 6), the empirical optimal range $p_2 \in [0.7, 0.8]$ contrasts with our theoretical prediction that smaller p_2 values should yield faster convergence through the bound $T \leq \frac{V(0)^{1-\gamma_1}}{\alpha_1(1-\gamma_1)}$ where $\gamma_1 = \frac{1+p_2}{2}$. This discrepancy reflects the inherent tension between theoretical acceleration and discrete-time stability in stochastic settings.

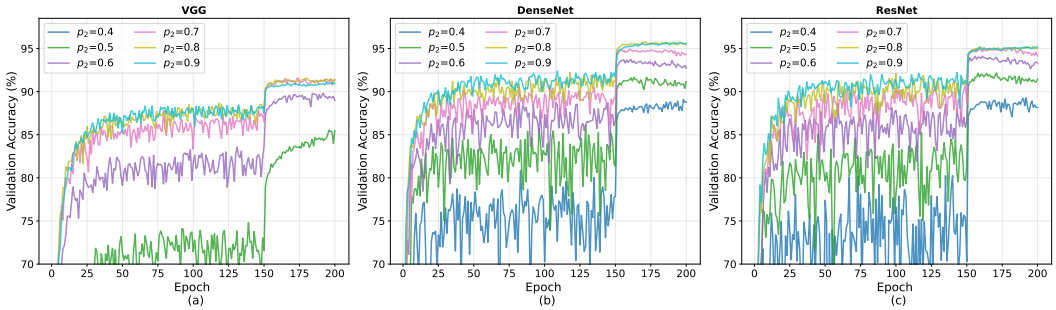

Figure 5: Test accuracy for CIFAR10 with different p_2 using PEFToM

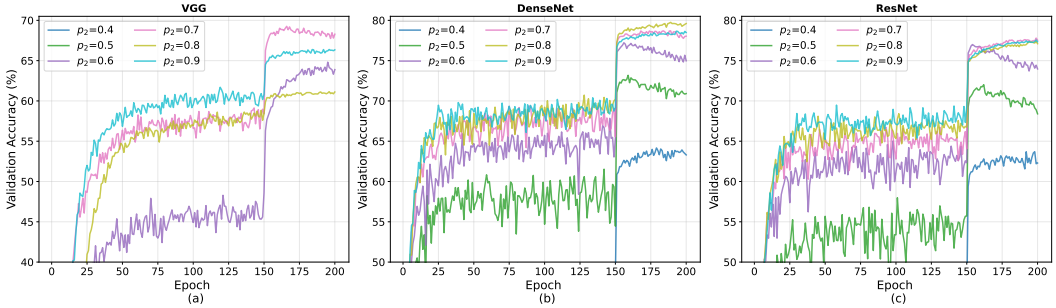

Figure 6: Test accuracy for CIFAR100 with different p_2 using PEFToM

Remarkably, C4 language modeling (Figure 7) exhibits the opposite pattern: smaller p_2 values achieve superior performance, with $p_2 = 0.2$ reaching the lowest validation loss while $p_2 \geq 0.4$ show limited convergence. This aligns more closely with our theoretical predictions, suggesting that optimal finite-time parameter selection depends critically on task-specific optimization landscape characteristics.

The vision-language dichotomy may reflect fundamental differences in gradient structure: language modeling's sparse, structured gradients may benefit from aggressive finite-time dynamics ($p_2 = 0.2, 0.3$), while vision tasks' dense, homogeneous gradients require more conservative parameters to balance acceleration with stability. On CIFAR-10, the simpler optimization surface tolerates broader parameter ranges, while CIFAR-100's complexity exposes sensitivity where $p_2 = 0.4, 0.5$ exhibit volatility and $p_2 = 0.9$ suffers late-stage instability.

Architecture-dependent responses provide additional insights into parameter sensitivity patterns. DenseNet demonstrates relative robustness across parameter choices, which may relate to its connectivity structure, while VGG shows pronounced sensitivity. These findings underscore the importance of joint task-architecture-aware parameter selection in finite-time optimization methods.

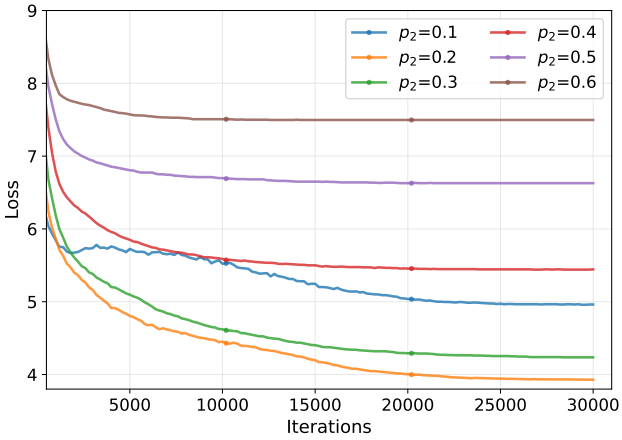

Figure 7: Test loss for C4 with different p_2 using EFToM